International Geology Review

Age, petrogenesis and tectonic significance of the ferrobasalts in the Chagangnuoer iron deposit, western Tianshan

Ning-Bo Li[ab], He-Cai Niu[a], Xing-Chun Zhang[c], Qiao-Song Zeng[a], Qiang Shan[a], Cong-Ying Li[a], Shuang Yan[ab] & Wu-Bin Yang[a]

[a] CAS Key Laboratory of Mineralogy and Metallogeny, Guangzhou Institute of Geochemistry, Chinese Academy of Sciences, Guangzhou, China

[b] University of Chinese Academy of Sciences, Beijing, China

[c] State Key Laboratory of Ore Deposit Geochemistry, Institute of Geochemistry, Chinese Academy of Sciences, Guiyang, China
Published online: 13 Feb 2015.

PLEASE SCROLL DOWN FOR ARTICLE

Taylor & Francis
Taylor & Francis Group

Age, petrogenesis and tectonic significance of the ferrobasalts in the Chagangnuoer iron deposit, western Tianshan

Ning-Bo Li[a,b], He-Cai Niu[a]*, Xing-Chun Zhang[c], Qiao-Song Zeng[a], Qiang Shan[a], Cong-Ying Li[a], Shuang Yan[a,b] and Wu-Bin Yang[a]

[a]*CAS Key Laboratory of Mineralogy and Metallogeny, Guangzhou Institute of Geochemistry, Chinese Academy of Sciences, Guangzhou, China;* [b]*University of Chinese Academy of Sciences, Beijing, China;* [c]*State Key Laboratory of Ore Deposit Geochemistry, Institute of Geochemistry, Chinese Academy of Sciences, Guiyang, China*

The formation of large iron deposits associated with subduction and its genetic relationships with ferrobasalts are not yet well understood. Here we report a geochemical and geochronological investigation on the newly discovered ferrobasalts associated with the Chagangnuoer iron deposit, western Tianshan. The Chagangnuoer ferrobasalts are characterized by high $Fe_2O_3{}^T$ (14.55–22.68 wt.%) and MnO (0.36–0.93 wt.%) but low TiO_2 (0.70–1.26 wt.%) contents. Analyses of 10 zircon grains yield a weighted zircon U–Pb age of 314 ± 8 Ma. Based on our new petrological and geochemical data, we conclude that the Chagangnuoer ferrobasalts probably have been originated from the partial melting of a spinel peridotite mantle source that has been modified by subduction related fluids. The ferrobasalts have nearly linear positive correlation between MnO and $(^{87}Sr/^{86}Sr)_i$, implying the involvement of subducted Fe–Mn nodules. The mid-ocean ridge basalt (MORB)- and ocean island basalt (OIB)-like geochemical features, as well as moderate Ti/V values (18–36), indicate that the ferrobasalts may have been formed in an extensional back-arc basin setting. Combined with previous studies on the Chagangnuoer iron deposit, we propose a hypothesis that the overlying iron orebodies were likely derived from the ferrobasaltic magma.

Keywords: ferrobasalt; back-arc basin; Chagangnuoer iron deposit; western Tianshan; subduction-modified lithospheric mantle

1. Introduction

Major ferrobasalts occurring in Precambrian strata are thought to have resulted from a much higher iron content in the Precambrian mantle than in the modern one (Francis *et al.* 1999). Minor Phanerozoic ferrobasalts are attributed to mantle plume activities (Ichiyama *et al.* 2006). In general, subduction zones have high oxygen fugacity (fO_2) (Sun *et al.* 2007, 2013, 2015; Evans *et al.* 2012; Kelley and Cottrell 2012; Berry *et al.* 2013) and are rich in H_2O content (Tatsumi *et al.* 1986; Kelley and Cottrell 2009) that may hinder the iron enrichment (e.g. Kawamoto and Holloway 1997; Gibson 2002; Xu *et al.* 2003; Peng *et al.* 2013). This may be the key reasons for ferrobasalts being particularly rare in subduction zones. However, recent studies have revealed that subduction processes can introduce basaltic crust components into the peridotitic mantle (Sobolev *et al.* 2007; Marschall and Schumacher 2012), and the partial melting of such a mixture source may produce iron-rich melts (Kogiso *et al.* 1998). In addition, involvement of recycled iron-rich components (e.g. Baker and Krogh Jensen 2004) and subduction-related fluids may leach iron from the subducted slab and mantle wedge during their ascent (Li *et al.* 2013; Ling *et al.* 2013) and would thus also facilitate the formation of such iron-rich melts.

Because the density of the iron-rich magma is higher than that of the 'normal' basaltic magma, extensional environments, such as continental rifts (Xu *et al.* 2003; Peng *et al.* 2007; Zhang *et al.* 2012b), middle ocean ridges (Leroex *et al.* 1982; Brooks *et al.* 1991), post-collision extensional settings (Wang *et al.* 2004, 2008), and back-arc basins (Leybourne *et al.* 1999; Kerrich *et al.* 2008), are required to transport the iron-rich magmas to the Earth's surface. Although iron-rich rocks rarely appear on the surface (Fisk 1986; Brooks *et al.* 1991), their mineralization potential has been discussed previously (e.g. Zhou *et al.* 2005; Kerrich *et al.* 2008; Zhang *et al.* 2009). Kerrich *et al.* (2008) reported that the ferrobasalts in the Abitibi and Wawa greenstones are spatially and temporarily associated with volcanogenic massive sulphide (VMS) deposits. Zhou *et al.* (2005) and Zhang *et al.* (2009) proposed that the parental magma of the Fe–Ti–V oxide ore-bearing intrusions in the Panzhihua area, Southwest China, requires a source of iron-rich gabbro in composition. However, the contribution of the ferrobasalts to the formation of iron deposit is not yet well understood.

Late Palaeozoic volcanic rocks and associated iron deposits are widely distributed in the Awulale Mountains, western Tianshan (Shan *et al.* 2009; Wang *et al.* 2011; Hong *et al.* 2012a; Zhang *et al.* 2012a, 2014b; Hou *et al.* 2014).

However, the tectonic settings of these volcanic rocks and the metallogenesis of these iron deposits are still controversial. The major debates focus on the time of regional geodynamic transformation from subduction to intraplate settings (Zhu *et al.* 2006a, 2006b; Yang *et al.* 2012, 2014a) and whether these deposits belong to magmatic deposits (Zhang *et al.* 2012a, 2014b, 2014c, 2014d; Duan *et al.* 2014; Hou *et al.* 2014; Jiang *et al.* 2014). Therefore, detailed studies of the volcanic rocks that related to iron mineralization can provide critical evidence for reconstructing the regional tectonic evolution and metallogenesis. In this study, we have newly identified a suite of ferrobasalts in the Chagangnuoer iron deposit area, in the eastern segment of the Awulale Mountains. An integrated study on zircon U–Pb geochronology, whole rock geochemistry, and Sr–Nd

isotopes of the ferrobasalts was carried out to constrain their mantle-source nature and probable tectonic setting, together with their metallogenic contribution to the Chagangnuoer iron deposit.

2. Local geology and petrography

The Central Asia Orogenic Belt (CAOB) is one of largest accretionary orogens (Şengör *et al.* 1993; Windley *et al.* 2007; Cawood *et al.* 2009; Xiao *et al.* 2009, 2010, 2013) and one of the most significant metallogenic belts in the world (Heinhorst *et al.* 2000; Xiao *et al.* 2009, 2013). Western Tianshan is located in the southwestern part of the CAOB and sandwiched between the Tarim plate to the south and the Junggar basin to the north (Figure 1(a)).
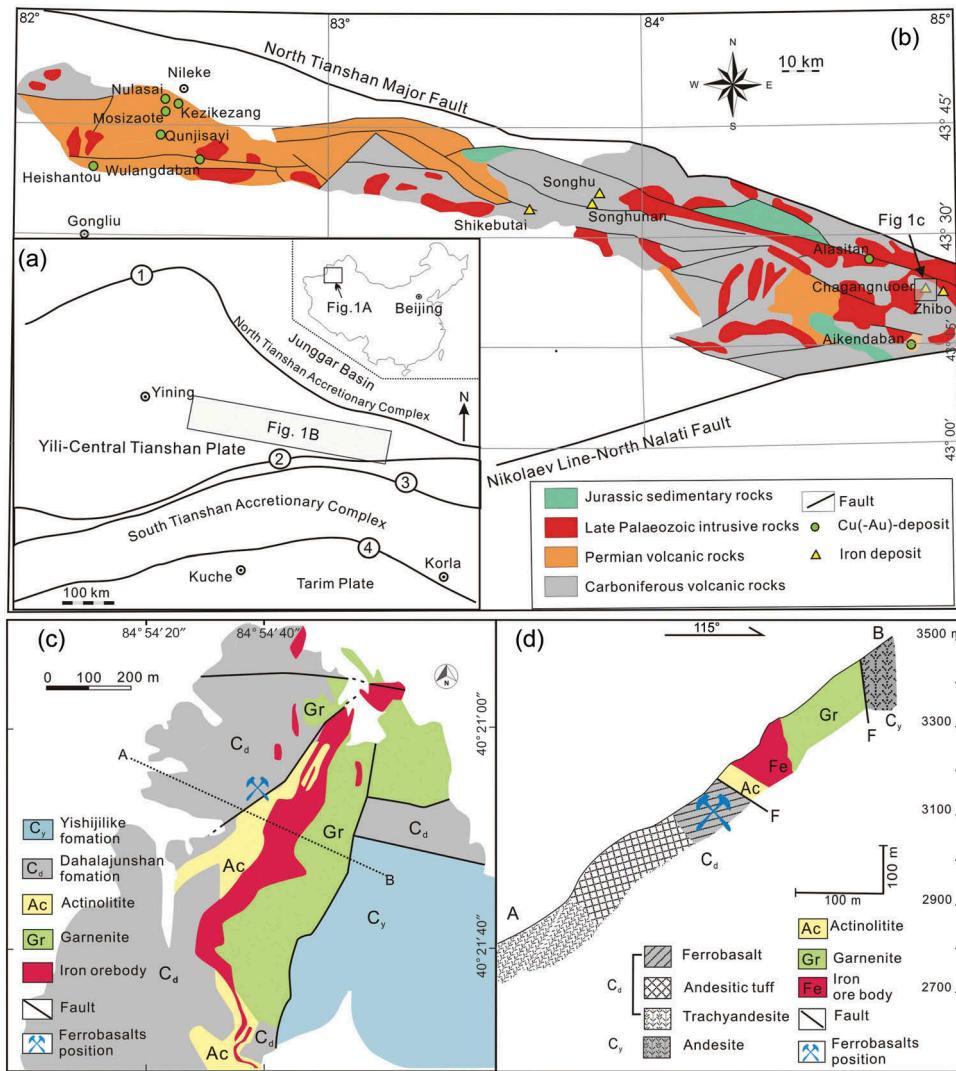
Figure 1.   (a) Tectonic sketch map of the Western Tianshan (modified from Gao *et al.* 2009; 1, North Tianshan Fault; 2, Nikolaevline–North Nalati Fault; 3, South Nalati–Qawabulak Fault; 4, South Tianshan Fault). (b) Simplified tectonic-geological sketch map of the Awulale Mountains (modified from Zhao *et al.* 2000). (c) Simplified geological map of Chagangnuoer area. (d) A geological profile of line A–B across the Chagangnuoer iron orebody.

Traditionally, the western Tianshan is subdivided into three parts, namely the South Tianshan Accretionary Complex (STAC), the Yili-Central Tianshan Plate (YCTP), and the North Tianshan Accretionary Complex (NTAC) (Figure 1(a); Wang *et al.* 1990; Allen *et al.* 1993; Gao *et al.* 2009). The NTAC is the main tectonic unit in the northern edge of the western Tianshan and separates the Junggar Basin in the north from the YCTP in the south. The complex comprises late Carboniferous to Permian post-collision-related granitoid plutons and early Carboniferous ophiolitic mélanges (Han *et al.* 2010 and references therein). The ophiolitic mélanges occur along the North Tianshan fault and represent the final closure of the North Tianshan Ocean (Xiao *et al.* 2004, 2013; Han *et al.* 2010). A plagiogranite from the ophiolitic mélanges has yielded a zircon U–Pb age of 325 Ma (Xia *et al.* 2004b; Xu *et al.* 2006). The YCTP, also known as Yili-Central Tianshan Arc, is situated between the Nikolaevline–North Nalati Fault and North Tianshan Fault (Figure 1(a)). Some researchers suggest that the YCTP is a Precambrian micro-continental block rifted from the Tarim plate (Chen *et al.* 1999; Shu *et al.* 2011), whereas other researchers suggest that the YCTP is an independent block (Xiao *et al.* 2013 and references therein). The YCTP is mainly composed of Proterozoic to Silurian sedimentary–metamorphic rocks and the overlying late Palaeozoic volcano-sedimentary strata. The Late Devonian–early Carboniferous STAC is the border of the Tarim plate and YCTP and formed by closure of the South Tianshan Ocean. The initial closure of the South Tianshan Ocean may have been diachronous and was becoming generally younger westwards (Chen *et al.* 1999; Xiao *et al.* 2004, 2013).

The Awulale Mountains are located in the eastern part of the YCTP (Figure 1(a)) and mainly composed of Carboniferous and Permian igneous rocks (Wang *et al.* 1990; Allen *et al.* 1993; Gao *et al.* 2009). Due to the extensive occurrences of numerous Fe–Cu (Au) deposits, the Awulale Mountains are also known as the Awulale Fe–Cu (Au) Metallogenetic Belt (AMB) (Zhang *et al.* 2012a). It is noted that the Cu (Au) deposits are mostly distributed in the western AMB and related to the Permian igneous rocks, whereas iron deposits are mostly distributed in the central and eastern AMB and related to the Carboniferous igneous rocks (Figure 1(b)). Hou *et al.* (2014) proposed that the metallogenesis of these iron deposits was associated with submarine volcanism. These iron deposits can be subdivided into two series according to their host rock types. One is a volcano-sedimentary rock-hosted type, including Songhu, Songhunan, and Shikebutai iron deposits (Shan *et al.* 2009). The other is a volcanic-hosted type, including the Chagangnuoer, Zhibo, Dunde, and Beizhan iron deposits (Feng *et al.* 2010; Duan *et al.* 2014; Hou *et al.* 2014; Jiang *et al.* 2014). Major rock units exposed at the Chagangnuoer area include the Carboniferous Yishijilike (C_y) and Dahalajunshan (C_d) formations (Figure 1(c)). The Yishijilike Formation is composed of basaltic andesite, rhyolitic tuff, and limestone, whereas the Dahalajunshan Formation is composed of basalt, andesitic basalt and tuff, dacite, and rhyolitic tuff. Feng *et al.* (2010) reported a rhyolite in the Dahalajunshan Formation, with a zircon U–Pb age of 321 ± 1 Ma. Both the ferrobasalts and the iron orebodies in the Chagangnuoer area are hosted in the upper part of the Dahalajunshan Formation (Figure 1(d)). The ferrobasalts present as lava and are sandwiched between the orebody and andesitic tuff. The ferrobasalts generally have sharp contacts with the andesitic tuff and the orebody (Figure 1(c) and 1(d)).

The ferrobasalts in the Chagangnuoer area are characterized by a porphyritic texture (Figure 2) with phenocrysts of pyroxene (45–60%) and hornblende (25–40%) (Figure 2(a)), and a matrix of plagioclase (48–52%), pyroxene (6–8%),
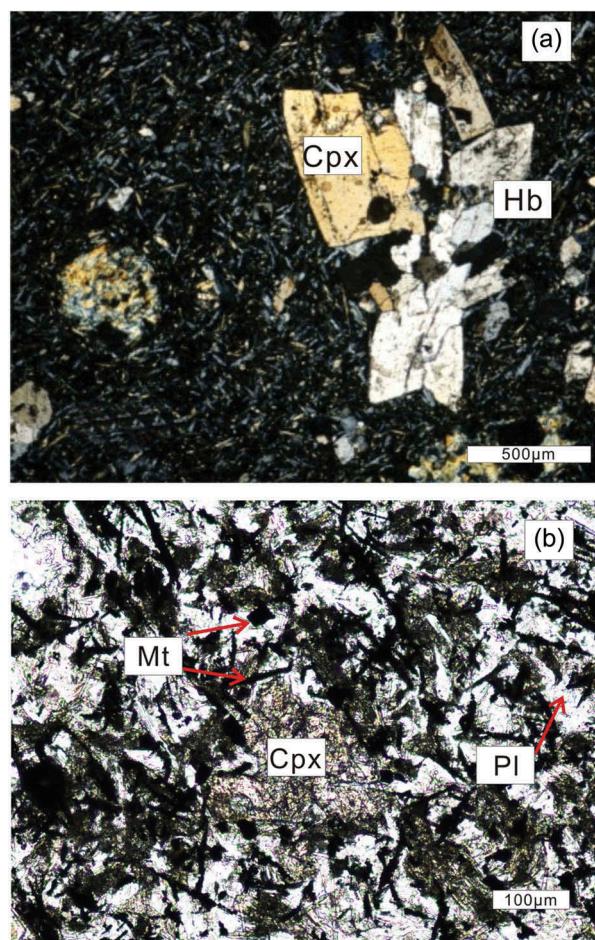

Figure 2. Micrographs of the Chagangnuoer ferrobasalts. (a) Sample CGB-5 (cross-polarized light), showing euhedral pyroxene and hornblende phenocrysts. (b) Sample CGB-1 (plane-polarized light), showing magnetite clusters in the matrix. (Cpx: clinopyroxene, Hb: hornblende, Mt: magnetite, Pl: Plagioclase).

hornblende (10–14%), and magnetite (14–16%) (Figure 2(b)). Plagioclase, pyroxene, and hornblende are partly altered to epidote, chlorite, and actinolite.

3. Analytical methods

3.1. Zircon U–Pb dating

Zircon grains were separated from an approximately 12 kg ferrobasalt sample using standard density and magnetic separation techniques and handpicking. Representative zircon crystals were mounted in an epoxy mount, and were then polished to near half-thickness. After that, all zircon grains on the mount were studied with transmitted and reflected light microscopy, as well as cathodoluminescence (CL) for revealing their external and internal structures. Zircon U–Pb analyses were carried out on an Agilent 7500a inductively coupled plasma mass spectrometer (ICP-MS) coupled with an excimer laser ablation (LA) system (Resonetics Resolution 50) at the State Key Laboratory of Isotope Geochemistry, Guangzhou Institute of Geochemistry, Chinese Academy of Sciences (GIGCAS), using a He carrier gas and a laser beam diameter of 32 μm. The zircon standard TEMORA 2 (Black et al. 2004) was used as the external standard for the dating. The zircon standard was analysed twice in every batch of five analyses in order to ensure the accuracy of the results. The analytical procedures are described by Tu et al. (2011) and Li et al. (2012a). The isotopic ratios and trace element contents of the zircons were calculated by using GLITTER 4.0 software (Macquarie University, Australia). The U–Pb ages were calculated by using ISOPLOT 4.11 (Ludwig 2008).

3.2. Whole rock geochemistry analyses

Samples of the Chagangnuoer ferrobasalt were examined first using optical microscopy. Only the unaltered or least-altered samples were selected for further studies. Major and trace elements were analysed in the State Key Laboratory of Isotope Geochemistry, GIGCAS. Major elements were analysed using a conventional X-ray fluorescence method following the standard procedures described by Li et al. (2005), with less than 5% analytical deviation for most elements. Trace elements were determined using a Perkin-Elmer ELAN 6000 ICP-MS following procedures described in detail by Li (1997), with less than 3% analytical deviation for most elements.

The Sr and Nd isotopic compositions of the ferrobasalt samples were analysed using a Micromass Isoprobe multicollector mass spectrometer at GIGCAS, following procedures described by Wei et al. (2002) and Liang et al. (2003). The mass fractionation corrections for Sr and Nd isotopic ratios are based on a $^{86}Sr/^{88}Sr$ ratio of 0.1194 and $^{146}Nd/^{144}Nd$ ratio of 0.7219, respectively. The $^{87}Sr/^{86}Sr$ ratio of the Standard NBS SRM 987 and the $^{143}Nd/^{144}Nd$ ratio of the Standard Shin Etsu JNdi-1 determined during this study were 0.71025 and 0.512115, respectively.

4. Results

4.1. Zircon U–Pb geochronology

The zircon U–Pb ages yielded from the Chagangnuoer ferrobasalts are listed in Table 1 and illustrated in a concordia diagram (Figure 3). All zircon grains are transparent, light yellow brown and prismatic, with obvious oscillatory zoning in CL images (Figure 3). The Th/U values of 0.51–1.34 (Table 1) indicate that these zircons are of typical magmatic origin (Hoskin and Black 2000; Belousova et al. 2002; Yang et al. 2014b). The $^{206}Pb/^{238}U$ ages of the 10 analyses range from 302 ± 4 Ma to 334 ± 34 Ma (Table 1), with a weighted average age of 314 ± 8 Ma (Figure 3).

Table 1. Zircon U–Pb isotopic data of the Chagangnuoer ferrobasalts.

| Analysis spots	Concentrations and ratios			Isotopic ratios						Apparent ages (Ma)			
	Th (ppm)	U (ppm)	Th/U	$^{207}Pb/^{206}Pb$	1σ	$^{207}Pb/^{235}U$	1σ	$^{206}Pb/^{238}U$	1σ	$^{207}Pb/^{235}U$	1σ	$^{206}Pb/^{238}U$	1σ
CGB-2@01	376	456	0.83	2.0066	0.2485	1.3945	0.0811	0.0506	0.0013	887	34	318	8
CGB-2@02	55	108	0.51	1.3528	0.2503	0.9385	0.1549	0.0498	0.0035	672	81	313	21
CGB-2@03	897	860	1.04	0.4581	0.0675	0.3123	0.0421	0.0488	0.0016	276	33	307	10
CGB-2@04	80	70	1.13	0.5415	0.2623	0.4033	0.1906	0.0532	0.0056	344	138	334	34
CGB-2@05	42	65	0.64	0.7296	0.1895	0.5019	0.1246	0.0491	0.0033	413	84	309	20
CGB-2@06	86	133	0.65	1.1064	0.1421	0.8008	0.0913	0.0514	0.0023	597	51	323	14
CGB-2@07	35	59	0.59	1.1927	0.2160	0.8277	0.1202	0.0506	0.0019	612	67	318	12
CGB-2@08	50	72	0.69	0.4582	0.1822	0.3011	0.1153	0.0479	0.0023	267	90	302	14
CGB-2@09	33	63	0.52	0.7387	0.1491	0.5007	0.0877	0.0494	0.0018	412	59	311	11
CGB-2@10	119	89	1.34	0.5978	0.1802	0.4107	0.1183	0.0498	0.0028	349	85	313	17
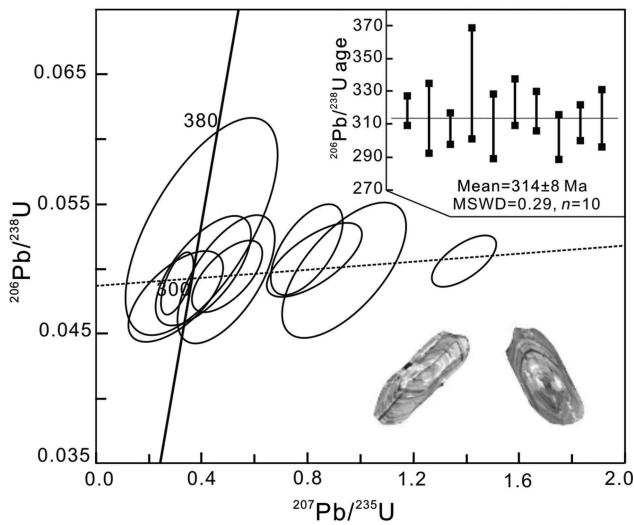
Figure 3. Zircon U–Pb concordia age diagram for the Chagangnuoer ferrobasalts.

4.2. Geochemistry of the ferrobasalts

Major and trace element compositions of the Chagangnuoer ferrobasalts are listed in Table 2. The samples vary in SiO_2 (43.11–54.27 wt.%), $Fe_2O_3^T$ (14.55–22.68 wt.%), TiO_2 (0.70–1.26 wt.%), MgO (5.63–7.7 wt.%), MnO (0.36–0.93 wt.%), and total alkalis (1.00–5.22 wt.%). On the $(Fe_2O_3^T + TiO_2)$–Al_2O_3–MgO diagram, the rocks are classified as high-iron tholeiitic basalt (Figure 4). The ferrobasalts have significantly higher $Fe_2O_3^T$ and MnO than those of the basalts from the worldwide convergent margins (Figure 5(a) and 5(b)). In addition, compared to the iron-rich unit ($Fe_2O_3^T > 14$ wt.%) of continental flood basalts, the Chagangnuoer ferrobasalts are rich in MnO but obviously poor in TiO_2 (Figure 5(c) and 5(d)). Their Cr, Co, Ni, and V contents are 26–617 ppm, 163–229 ppm, 80–243 ppm, and 130–229 ppm, respectively. Their total rare earth element (REE) concentrations vary from 23.5 to 68.5 ppm, with $(La/Sm)_N$, $(La/Yb)_N$, $(Dy/Yb)_N$, and δEu values of

Table 2. Geochemical compositions of the Chagangnuoer ferrobasalts.

Sample	CGB-1	CGB-2	CGB-3	CGB-4	CGB-5	CGB-6	CGB-7	CGB-8	CGB-9	CGB-10	CGB-11	CGB-12	CGB-13	CGB-14
SiO_2	48.12	45.7	44.19	51.07	43.11	44.75	50.39	45.48	47.19	44.77	46.4	45.49	43.42	54.27
TiO_2	1.13	0.98	0.89	0.87	0.72	0.94	0.92	1.26	0.77	1.25	1.06	0.84	0.7	0.85
Al_2O_3	14.40	11.64	11.36	14.25	9.43	10.87	10.62	13.87	12.78	13.92	12.87	12.33	9.01	13.93
$Fe_2O_3^T$	14.55	20.79	21.79	16.85	22.68	21.92	15.89	18.21	17.85	18.93	17.42	19.42	21.13	15.39
MnO	0.55	0.39	0.47	0.65	0.36	0.51	0.93	0.42	0.51	0.48	0.50	0.66	0.55	0.60
MgO	6.22	6.13	6.70	6.99	7.35	6.67	7.70	5.63	5.73	5.63	6.63	7.38	7.61	6.16
CaO	7.20	8.56	9.15	3.44	12.13	8.77	6.12	9.57	7.61	9.53	7.17	7.61	13.38	3.30
Na_2O	2.26	1.83	1.62	0.41	0.93	1.17	2.12	2.08	1.99	1.94	1.77	2.51	0.95	0.26
K_2O	2.96	2.17	1.70	0.75	1.82	2.09	2.83	1.62	2.74	1.66	2.78	0.82	1.55	0.74
P_2O_5	0.23	0.21	0.16	0.40	0.13	0.13	0.08	0.22	0.10	0.22	0.20	0.17	0.14	0.42
L.O.I	2.20	1.39	1.73	4.26	1.12	1.74	2.28	1.53	2.26	1.59	2.75	2.36	1.44	3.85
Total	100.05	99.93	99.87	99.94	99.80	99.56	99.87	99.91	51.57	99.91	52.08	99.59	99.88	99.77
Sc	/	/	/	33.5	30.1	29.7	29.9	28.3	24.8	29.5	30.8	30.5	33.3	31.3
Ti	6780	5880	5340	5391	4862	5510	5150	7389	4632	7455	6325	4570	4452	5012
V	210	163	215	229	185	191	168	212	130	199	199	218	187	202
Cr	250	300	320	236	617	230	25.7	163	80.3	150	222	302	596	243
Co	20.6	13.2	40.1	70.4	45.8	25.3	17.7	30.3	12.8	18.2	17.3	14.4	40.5	71.8
Ni	27.3	15.4	34.2	66.1	43.2	19.5	9.53	40.1	6.78	40.5	26.9	39.8	36.6	67.9
Cu	5.32	4.86	72.2	11.4	29.6	236	5.81	13.9	11.1	30.9	85.6	30.4	58.1	8.50
Zn	194	109	189	232	197	113	229	152	115	162	119	161	153	212
Ga	13.9	11.4	14.3	16.7	13.8	12.8	12.7	12.9	11.2	12.9	12.5	12.8	14.6	16.0
Ge	/	/	/	1.88	1.86	1.39	3.27	1.34	1.48	1.42	1.51	1.6	1.93	1.66
Rb	71.5	37.4	36.1	27.9	32.9	42.1	63.1	57.5	57.8	57.5	72.5	12.1	30.7	27.7
Sr	180	111	93.2	223	67.3	76.1	21.9	178	153	159	142	100	51.2	182
Y	20.1	12.2	13.6	17.3	13.2	13.1	25.1	19.3	18.3	18.1	17.4	14.9	14.9	16.5
Zr	100	80.4	65.4	112	57.8	72.7	70.7	97.8	75.6	100	83.4	62.2	59.9	104
Nb	4.72	3.64	2.84	4.45	2.52	3.26	2.49	4.78	3.22	4.83	3.89	2.56	2.48	4.32
Cs	0.53	0.31	0.34	/	/	1.43	1.22	1.68	1.67	2.15	1.19	0.18	0.38	/
Ba	1545	730	476	112	326	624	392	290	1377	311	1131	233	373	113
La	3.71	3.63	2.32	9.41	3.93	1.55	2.91	2.79	5.19	2.18	3.39	2.16	2.1	10.3
Ce	12.4	11.1	5.81	21.1	9.71	5.96	9.76	11.7	13.6	8.83	14.8	8.01	9.15	22.8
Pr	2.01	1.68	0.92	3.13	1.55	1.08	2.31	2.14	2.19	1.67	2.69	1.37	1.67	3.39
Nd	9.51	7.72	4.73	14.1	7.39	5.52	12.9	10.5	10.4	8.63	12.5	6.66	8.33	15.1
Sm	2.83	1.86	1.51	3.45	2.06	1.66	4.02	2.95	2.78	2.62	3.13	1.84	2.29	3.67
Eu	0.55	0.51	0.27	0.82	0.69	0.25	0.83	0.54	0.69	0.44	0.74	0.37	0.48	0.90
Gd	3.06	2.08	1.77	3.36	2.31	1.93	4.42	3.09	3.06	2.86	3.19	2.12	2.52	3.59
Tb	0.58	0.37	0.35	0.56	0.36	0.38	0.81	0.57	0.55	0.53	0.53	0.39	0.43	0.55
Dy	3.54	2.03	2.21	3.34	2.57	2.35	5.08	3.46	3.43	3.29	3.23	2.51	2.70	3.39
Ho	0.73	0.44	0.47	0.66	0.53	0.49	1.07	0.72	0.72	0.67	0.67	0.58	0.59	0.69

(*Continued*)

Table 2.   (Continued).

Sample	CGB-1	CGB-2	CGB-3	CGB-4	CGB-5	CGB-6	CGB-7	CGB-8	CGB-9	CGB-10	CGB-11	CGB-12	CGB-13	CGB-14
Er	2.02	1.29	1.38	1.82	1.53	1.38	2.94	2.03	2.05	1.84	1.93	1.59	1.49	1.92
Tm	0.29	0.19	0.21	0.27	0.22	0.19	0.42	0.27	0.29	0.26	0.27	0.26	0.22	0.24
Yb	1.94	1.21	1.33	1.82	1.33	1.26	2.73	1.83	1.97	1.66	1.74	1.65	1.48	1.76
Lu	0.32	0.23	0.21	0.27	0.21	0.20	0.45	0.27	0.30	0.26	0.28	0.25	0.23	0.28
Hf	2.62	2.11	1.74	2.63	1.52	2.09	2.23	2.73	2.37	2.79	2.46	1.80	1.71	2.78
Ta	0.31	0.24	0.21	0.29	0.18	0.25	0.20	0.35	0.27	0.35	0.29	0.21	0.19	0.30
Pb	3.81	2.52	4.59	3.28	6.46	2.59	3.20	8.27	2.25	3.52	7.54	7.49	1.83	3.12
Th	1.89	1.54	1.34	3.63	1.93	1.72	1.80	2.06	2.49	2.12	1.98	1.97	1.50	3.44
U	0.88	1.39	0.48	1.30	2.23	0.78	1.19	1.29	1.82	1.67	1.38	0.88	0.67	1.22
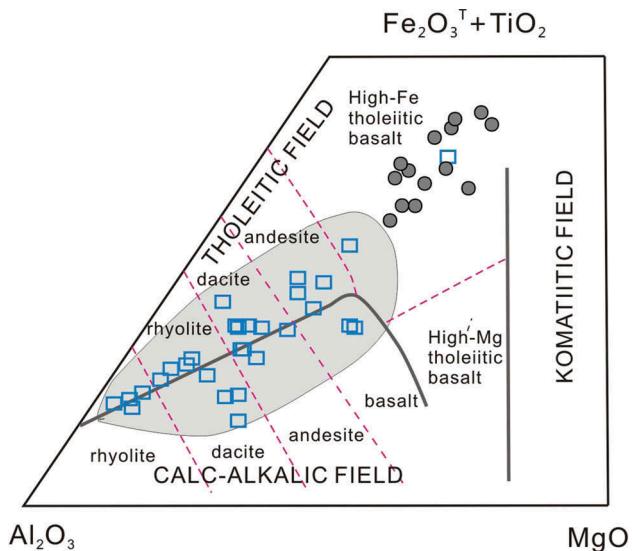
Figure 4. $(Fe_2O_3{}^T + TiO_2)$–Al_2O_3–MgO (Jensen 1976) classification diagrams of the Chagangnuoer ferrobasalts. The blue open squares representing data points of the Dahalajunshan Formation in the Chagangnuoer area are from Feng *et al.* (2010) and the black circles are the Chagangnuoer ferrobasalts.

0.43–0.97, 0.76–4.19, 1.06–1.69, and 0.47–1.80, respectively.

Initial (t = 314 Ma) Sr and Nd isotopic compositions of the Chagangnuoer ferrobasalts are presented in Table 3. The Chagangnuoer ferrobasalts have initial $^{87}Sr/^{86}Sr$ ratios varying from 0.704571 to 0.705776 and positive $\varepsilon_{Nd}(t)$ values varying from 1.58 to 4.74.

5.   Discussion

5.1.   *Petrogenesis*

5.1.1.   *Fractional crystallization and crustal contamination*

Both fractional crystallization and crustal contamination may cause geochemical and isotopic composition variations in the ferrobasalts during the magma ascent. Therefore, it is necessary to assess the possible geochemical impacts of these factors on the evolution of the ferrobasaltic magma. The positive MgO *versus* Ni correlation (Figure 6(a)) is consistent with the fractional crystallization of olivine and/or clinopyroxene. However, the CaO/Al_2O_3 values remain approximately unchanged with decreasing MgO (Figure 6(b)), indicating that clinopyroxene was not a major fractional crystallization phase (e.g. Mayer *et al.* 2013). Negative MgO *versus* P_2O_5 and TiO_2 (Figure 6(c) and 6(d)) correlation infer that the apatite and Ti-oxide fractionation was insignificant (e.g. Wang *et al.* 2008). Therefore, the P and Ti depletions in the Chagangnuoer ferrobasalts (Figure 7(a)) may represent their source geochemistry (e.g. the presence of rutile/titanite) (Ding *et al.* 2009, 2013; Liang *et al.* 2009; Xiong *et al.* 2011), which is typical at convergent margins. The lacking of negative Eu anomalies in the chonderited-normalized REE distribution patterns (Figure 7(b)) and negative MgO *versus* Al_2O_3 correlation (Figure 6(e)) suggest that plagioclase was not a major fractional crystallization phase (e.g. Mayer *et al.* 2013). This is supported by the negative Sr *versus* MgO correlation (Figure 6(f)) and negligible negative Sr anomaly (except CGB-7) in the primitive mantle-normalized spider diagram (Figure 7(a)). In addition, the Chagangnuoer ferrobasalts contain considerable accounts of hornblende, implying a water-rich parental magma. Previous experimental studies have demonstrated that plagioclase crystallization may be significantly delayed in hydrous ferrobasaltic melts (Botcharnikov *et al.* 2008). Thus, the aforementioned geochemical signatures of the Chagangnuoer ferrobasalts suggest that their parental magma may have undergone obviously fractional crystallization of olivine with minor clinopyroxene, apatite, Ti-oxide, and plagioclase.

The Th/U values of the Chagangnuoer ferrobasalts (0.87–2.82) are lower than those of mid-ocean ridge basalt (MORB) (ca. 3.0), ocean island basalt (OIB) (ca. 3.4), and upper-crustal rocks (ca. 5.0) (Rudnick and Fountain 1995), indicating that the basaltic magma was not significantly contaminated by crustal components (e.g. Wang *et al.* 2008). Continental crust is strongly depleted in high field strength elements (HFSEs) (Taylor and McLennan 1985). If the Ta depletion in the basalts is taken as evidence for crustal contamination, a positive correlation between
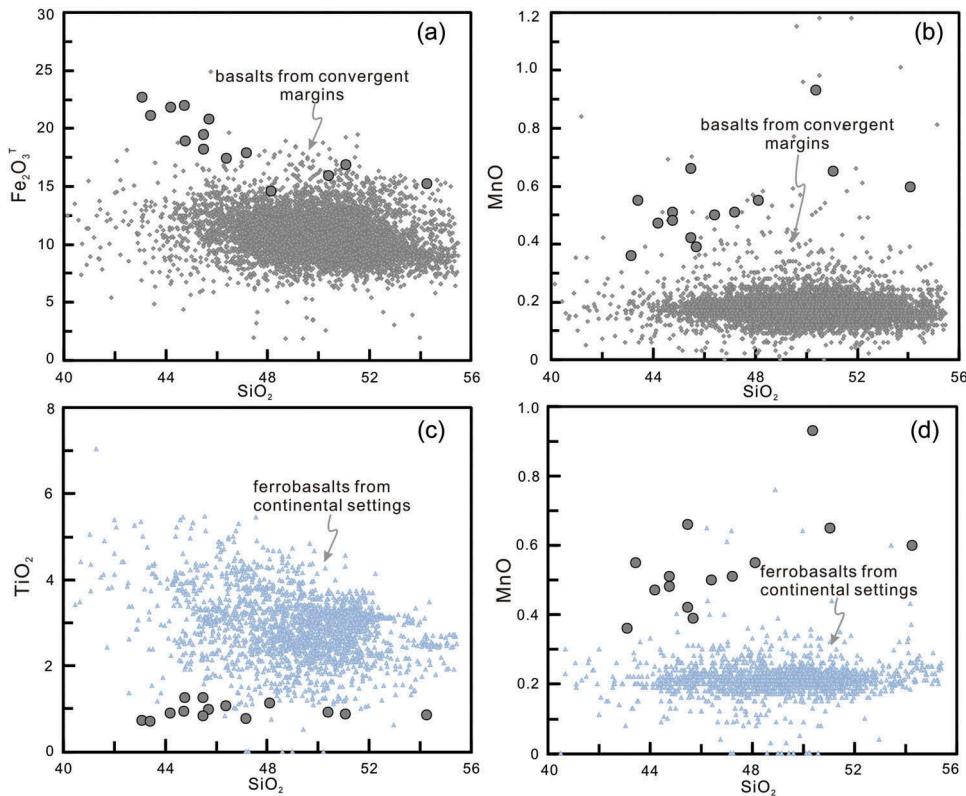
Figure 5. Harker diagrams for the Chagangnuoer ferrobasalts in comparison with the basalts from worldwide convergent margins (a and b) and ferrobasalts from worldwide continental settings (c and d). The data of typical convergent margin basalts and continental ferrobasalts are from http://georoc.mpch-mainz.gwdg.de/georoc/.

La/Ta and La/Sm would be expected because upper continental crust is enriched in LREEs, and partial melting of these rocks would further increase the La/Sm values of the resultant magmas (Lassiter and DePaolo 1997; Said and Kerrich 2010). The Chagangnuoer ferrobasalts have high La/Ta values, combined with relatively low and constant La/Sm values, suggesting that the basalts have not undergone significant crustal contamination (Figure 8). In addition, it has been argued that crustal contamination of a primary magma could cause an increase in fO_2, resulting in early magnetite crystallization, and consequently decreasing of the iron content in the contaminated magma (Xu *et al.* 2003). The high $Fe_2O_3^T$ contents of the Chagangnuoer ferrobasalts may thus be taken as additional evidence that the magma may not have been significantly contaminated by crustal materials.

5.1.2. *Nature of the mantle sources*

To minimize the fractional crystallization influence, isotopic compositions and ratios of the elements with similar distribution coefficients (e.g. Dy/Yb, La/Sm and Sm/Yb ratios) have been used to investigate the possible source of the Chagangnuoer ferrobasalts. The $(^{87}Sr/^{86}Sr)_i$ and $\varepsilon_{Nd}(t)$ values of the Chagangnuoer ferrobasalts plot near the

boundary between the OIB and the island arc volcanic fields, similar to the Carboniferous western Tianshan basalts (Figure 9(a)). The relatively elevated positive $\varepsilon_{Nd}(t)$ values could suggest that a depleted mantle end-member may have been involved in the magma formation, whereas the high $(^{87}Sr/^{86}Sr)_i$ and low positive $\varepsilon_{Nd}(t)$ values imply that a juvenile crustal end-member might also be present in the magma source (Faure and Mensing 2005). Geochemical characteristics of the Chagangnuoer ferrobasalts, such as enrichments in large ion lithophile elements (Sr, K, Rb and Ba), favour a lithospheric mantle rather than depleted mantle source in their source (e.g. Temizel *et al.* 2012; Yang *et al.* 2012). The $(Nb/Ta)_N$ ratios of the Chagangnuoer ferrobasalts are mostly <0.8, and the $(Zr/Hf)_N$ ratios are ~1.0, indicating their enriched mantle source (e.g. Yang *et al.* 2012). Mantle metasomatism is an important process for generating an enriched mantle source through dehydration and/or partial melting of subducted slabs (Class *et al.* 2000 and references therein). As seen in the following discussion, the geochemistry of the Chagangnuoer ferrobasalts argues for a mantle source affected by slab dehydration rather than by the melting of subducted sediments.

Previous mineral-aqueous fluid partitioning experiments (Brenan *et al.* 1995; Ayers 1998) have suggested that the slab-released hydrous fluid has low Th/U values

Table 3. Sr–Nd isotopic data of the Chagangnuoer ferrobasalts.

Sample	Rb	Sr	Sm	Nd	$^{87}Rb/^{86}Sr$	$^{87}Sr/^{86}Sr$	2σ error	$(^{87}Sr/^{86}Sr)_i$	$\varepsilon_{Sr}(t)$	$^{147}Sm/^{144}Nd$	$^{143}Nd/^{144}Nd$	2σ error	$(^{143}Nd/^{144}Nd)_i$	$\varepsilon_{Nd}(t)$	$T_{DM,1}$ (Ma)
CGB-4	27.9	223	3.45	14.1	0.36	0.707386	0.000012	0.705768	23	0.15	0.512695	0.000007	0.512392	3.06	1054
CGB-8	57.5	178	2.95	10.5	0.93	0.708735	0.000012	0.704571	6.2	0.17	0.512819	0.000008	0.512471	4.61	1150
CGB-9	57.8	153	2.78	10.4	1.09	0.709897	0.000009	0.705027	13	0.16	0.512647	0.000007	0.512316	1.58	1469
CGB-10	57.5	159	2.62	8.63	1.05	0.709278	0.000016	0.704616	6.8	0.18	0.512854	0.000010	0.512478	4.74	1494
CGB-11	72.5	142	3.13	12.5	1.48	0.711354	0.000013	0.704771	9.0	0.15	0.512783	0.000007	0.512473	4.64	898
CGB-14	27.7	182	3.67	15.1	0.44	0.707738	0.000011	0.705776	23	0.15	0.512690	0.000008	0.512389	3.01	1050

because U preferentially enters fluids relative to Th (Jiang *et al.* 2009). The low Th/U values (0.87–2.82) of the Chagangnuoer ferrobasalts indicate that the mantle source had been metasomatized by slab-derived fluids (e.g. Jiang *et al.* 2009). The metasomatized nature of the mantle source for the Chagangnuoer ferrobasalts is revealed in the Th/Yb *versus* Ba/La diagram (Figure 9(b)), as these two ratios may effectively distinguish the roles of sediment melts and fluids as metasomatising agents (Sun *et al.* 2004). In this diagram, the Chagangnuoer ferrobasalt data points lie roughly parallel to the Ba/La axis, indicating that the mantle source may have been previously metasomatized by aqueous fluids (Sun *et al.* 2004). The Sm/Yb ratio is sensitive to basaltic source mineralogy (e.g. Genç and Tüysüz 2010). In the La/Sm *versus* Sm/Yb diagram (Figure 9(c)), the Chagangnuoer ferrobasalts are plotted between the fractional melting curve and the batch melting curve of spinel peridotite, implying that the magma may have been derived from the partial melting of spinel peridotite (e.g. Genç and Tüysüz 2010).

5.1.3. *Iron enrichment mechanism*

The iron-rich rocks are generally formed in a low fO_2 condition because high fO_2 causes early fractional crystallization of magnetite. Given that Ce^{4+} is far more compatible in zircon, the Ce content in zircon is mainly controlled by the Ce^{4+}/Ce^{3+} ratio of the parental magma (Liang *et al.* 2006). More-oxidized magma will yield a higher Ce anomaly in the zircon due to Ce^{4+} being more compatible than Ce^{3+} in zircon (Trail *et al.* 2011). Ce^{4+}/Ce^{3+} ratios calculated from the Ce anomaly in zircon is often used to estimate the fO_2 of magma (Li *et al.* 2012a; Zhang *et al.* 2013a, 2014a). Based on experiments, Trail *et al.* (2011) proposed a $1/T$ (T was estimated for using the Ti-in-zircon thermometer) *versus* Ce anomaly (δ Ce) plot, which has been subdivided into four fields by three common mineral oxidation buffers, namely magnetite–haematite (MH), fayalite–magnetite–quartz (FMQ), and iron–wustite (IW), and can be used to estimate the oxidation state of the magma (Figure 10(a)). By plotting the Ti-in-zircon temperatures and the calculated Ce anomalies on the $1/T$ *versus* δ Ce plot, zircons from the Chagangnuoer ferrobasalts mainly fall between IW and FMQ (Figure 10(a)). In addition, four zircons from the adjacent area also yield relatively low fO_2. Therefore, we conclude that the oxidation state of the Carboniferous to early Permian igneous rocks in the Awulale Mountains is low. The low oxidation magmatism favours the formation of iron-rich rocks.

The mechanism for iron enrichment in basic igneous rocks is still controversial, with three major models being proposed: (1) partial melting of a normal mantle source at high pressure (e.g. Hirose and Kushiro 1993; Lassiter and DePaolo 1997), (2) 'Fenner' fractionation of primitive
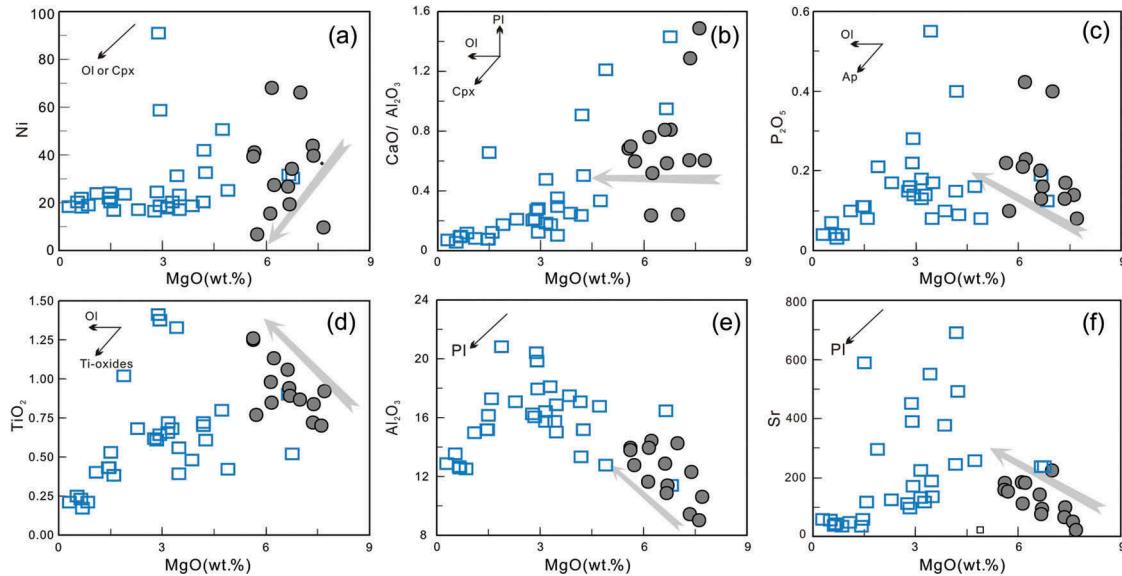
Figure 6. Variation diagrams of (a) Ni, (b) CaO/Al$_2$O$_3$, (c) P$_2$O$_5$, (d) TiO$_2$, (e) Al$_2$O$_3$, and (f) Sr *versus* MgO (as fractionation index) for the Chagangnuoer ferrobasalts. The grey arrows represent the fractionation trends of the ferrobasalts (symbols as in Figure 4).
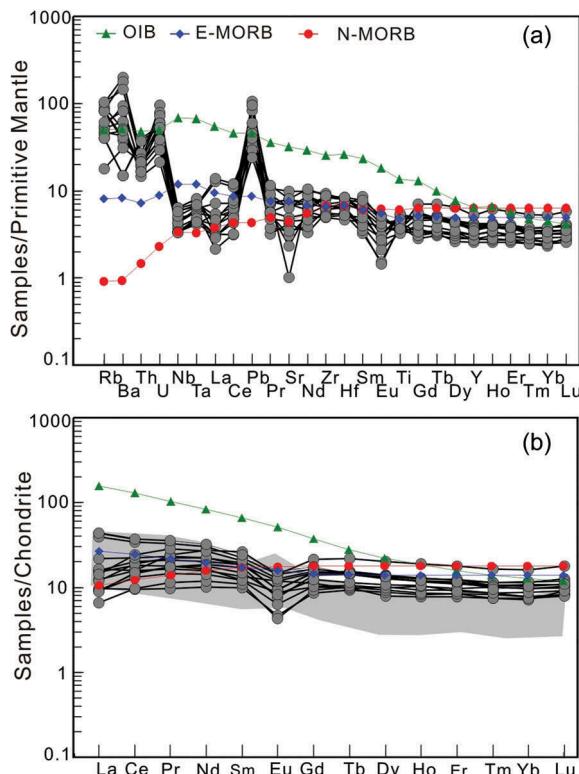
Figure 7. (a) Spider diagrams of trace elements and (b) REE distribution patterns for the Chagangnuoer ferrobasalts. Average primitive mantle, OIB, N-MORB, and E-MORB data are from Sun and McDonough (1989). The shaded field is the data for the magmatic magnetite from the Chagangnuoer iron deposit from Feng *et al.* (2010).
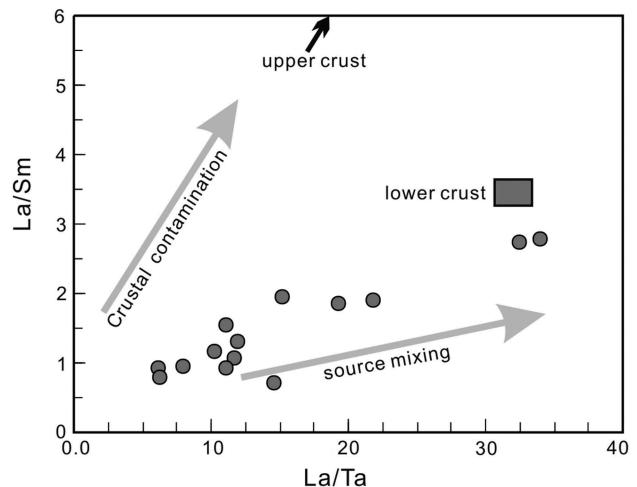
Figure 8. La/Sm *versus* La/Ta diagram showing the trends of crustal contamination and source mixing (after Lassiter and DePaolo 1997). Data of the upper and lower crust from Taylor and McLennan (1985).

magma (e.g. Leroex and Dick 1981; Leroex *et al.* 1982; Xu *et al.* 2003; Peng *et al.* 2013), and (3) mantle source inheritance (e.g. Kerrich *et al.* 1999; Gibson *et al.* 2000, 2002; Wang *et al.* 2004, 2008; Ichiyama *et al.* 2006). The Zr/Y and TiO$_2$/Al$_2$O$_3$ correlations have been used to estimate the partial melting pressure because for the peridotite-derived, TiO$_2$/Al$_2$O$_3$ increases linearly with increasing pressure (Ichiyama and Ishiwatari 2005; Ichiyama *et al.* 2006). The Tamba picritic ferrobasalts
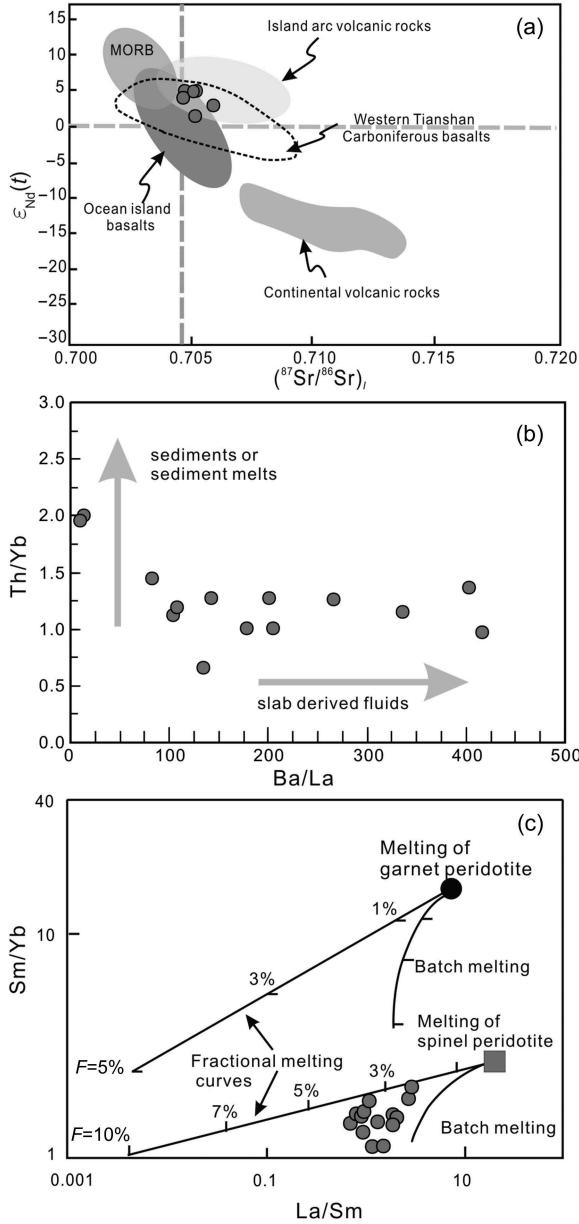
Figure 9. (a) $\varepsilon_{Nd}(t)$ *versus* $(^{87}Sr/^{86}Sr)_i$ diagram. Compositions of mid-ocean ridge basalt (MORB), ocean island basalt (OIB), island arc volcanic rocks, continental volcanic rocks, and western Tianshan Carboniferous basalts are from Hart *et al.* (1986), Zindler and Hart (1986), Hart *et al.* (1992), and Yang *et al.* (2012), respectively; (b) Th/Yb *versus* Ba/La diagram for the Chagangnuoer ferrobasalts. (c) Sm/Yb *versus* La/Sm diagram displaying the melting curves of the Chagangnuoer ferrobasalts (adopted from Genç and Tüysüz (2010) and Figure 19 of M. Keskin, http://www.mantleplumes.org/Anatolia.html).


Figure 10. (a) Magma oxidation of the Chagangnuoer ferroba-salts. For comparison, the data from adjacent areas are also shown, such as Songhu rhyolite (light blue rhombus, ca. 327 Ma) and tuff (black ×, ca. 305 Ma), Chagangnuoer dacite (blue triangles, ca. 313 Ma), and Yuximolegai quartz syenite porphyry (pink stars, ca. 284 Ma); (b) Zr/Y *versus* TiO_2/Al_2O_3 diagram for the Chagangnuoer ferrobasalts. The representative iron-rich mafic rocks from the Zhongtiao Mountains, Abitibi and Wawa (Kerrich *et al.* 2008) and the Tamba (Ichiyama *et al.* 2006) are also shown; and (c) $(^{87}Sr/^{86}Sr)_i$ *versus* MnO diagram for the Chagangnuoer ferrobasalts.

show higher Zr/Y and TiO_2/Al_2O_3 values than those of the Tamba ferropicrites (Figure 10(b)), suggesting that the partial melting of the former took place at a greater depth than the latter (Ichiyama *et al.* 2006). The Zr/Y and TiO_2/Al_2O_3 values of the Chagangnuoer ferrobasalts approach those of iron-rich mafic rocks generated in back-

arc basins, for example those preserved in the Zhongtiao Mountains (Li *et al.* 2014), and in the Abitibi and Wawa greenstone belts (Kerrich *et al.* 2008), implying that the melting pressure of Chagangnuoer ferrobasalts should be no greater than that of the iron-rich mafic rocks formed in back-arc basins. The negative SiO_2 *versus* $Fe_2O_3^T$ for the Chagangnuoer ferrobasalts (Figure 5(a)) suggests a magma evolution towards Si-rich and iron-poor, which is

in contrast to that for the 'Fenner' fractionation. It is widely accepted that plate tectonic subduction processes introduce basaltic crust (as eclogite) into the peridotitic mantle (Sobolev *et al.* 2007), and the melting experiments have revealed that the iron content of a melt derived from a peridotite–basalt mixture is higher than that of a melt derived from a pure peridotite (Kogiso *et al.* 1998). The production of a partial melt with FeO^T up to 20 wt.% would require a magma source with a peridotite–basalt mixture having a more than 50% basaltic component (Ichiyama *et al.* 2006). However, Sobolev *et al.* (2007) have estimated the amount of recycled crust in sources of mantle-derived melts and suggested the involvement of 2–20% (and up to 28%) of recycled crust. Partial melting of such a peridotite–basalt mixture (with ~30% basalt) may only produce a melt with up to 12 wt.% FeO^T (Kogiso *et al.* 1998), much lower than that of the Chagangnuoer ferrobasalts (14.55–22.68 wt.%). Therefore, we propose that the most reasonable explanation for the origin of the Chagangnuoer ferrobasalts was the partial melting of a subduction-modified mantle source with the recycling of iron-rich components.

Subduction of an oceanic crust containing Fe–Mn nodules into the mantle may account for the iron enrichment of the reconstructed sub-arc mantle (e.g. Baker and Krogh Jensen 2004). Partial melting of such an iron-enriched reconstructed mantle source may produce iron-rich melts with high $(^{87}Sr/^{86}Sr)_i$ and MnO (Ichiyama *et al.* 2006). The MnO contents of the Chagangnuoer ferrobasalts (0.36–0.93 wt.%) are higher than that of the majority of basalts on Earth (Figure 5(b) and 5(d)). In addition, there is an obvious linear positive correlation between the MnO (X) and $(^{87}Sr/^{86}Sr)_i$ (Y) of the Chagangnuoer ferrobasalts, indicating assimilations of Fe–Mn nodules during the partial melting of the spinel peridotite source (Figure 10(c)). This feature is consistent with the mantle source of the Chagangnuoer ferrobasalts undergoing source mixing (Figure 8). The average MnO content of depleted mantle is about 0.13 wt.% (Salters and Stracke 2004), consistent with that of the peridotite xenoliths in the Tuoyun area, western Tianshan (Zheng *et al.* 2006). When the MnO is 0.13 wt.%, the $(^{87}Sr/^{86}Sr)_i$ value of 0.7027 may represent the primary value of the mantle in western Tianshan. Therefore, it is inferred that the Chagangnuoer ferrobasalts with variable $(^{87}Sr/^{86}Sr)_i$ (0.704571–0.705776) and high MnO contents (0.36–0.93 wt.%) were derived from the partial melting of a mantle source with the incorporation of subducted Fe–Mn nodules.

5.2. Tectonic settings

The late Palaeozoic tectonic setting of the Awulale Mountains is still controversial: One hypothesis argues for a late Palaeozoic intra-continental rift (Che *et al.*

1996; Xia *et al.* 2004a) or a mantle plume (Xia *et al.* 2004b, 2008; Wang and Xu 2006), whereas another hypothesis proposes that the Carboniferous magmatism was subduction related, and the Permian magmatism was intraplate (Chen *et al.* 2004a, 2004b; Zhu *et al.* 2006a, 2006b, 2009; Gao *et al.* 2009; Su *et al.* 2011). Others suggest that continental or island arc settings related to subduction may have lasted until the late Permian–Triassic (Zhang *et al.* 2007; Xiao *et al.* 2010, 2013). It is widely accepted that the late Palaeozoic tectonic setting of the Awulale Mountains was mainly controlled by the northward subduction of the South Tianshan Ocean (e.g. Gao *et al.* 2009; Zhu *et al.* 2009; Yang *et al.* 2012; Zhang *et al.* 2012a; Xiao *et al.* 2013). Therefore, the key remaining tectonic issue is the closure time of the South Tianshan Ocean or the collision between the Tarim plate and YCTP. The collision is thought to have occurred during the Devonian–Carboniferous based on the age of associated ophiolitic mélanges (Charvet *et al.* 2007; Wang *et al.* 2011) or during the Carboniferous–Permian based on the occurrence of syn- and/or post-collision-related rocks (e.g. Gao *et al.* 2009; Long *et al.* 2011; Yang *et al.* 2012; Zhang *et al.* 2012a), or even during the Permian–Triassic based on tectonic reconstructions (Xiao *et al.* 2010, 2013) and the age of zircon from eclogites (Zhang *et al.* 2007).

For the mantle plume hypothesis, no Carboniferous large igneous province has been clearly identified in the Awulale Mountains, in which a great variety of volcanic rocks, including basalt, andesite, dacite, and rhyolite, with ages spanning across 50 million years have been documented (Zhu *et al.* 2009). The TiO_2 of the Chagangnuoer ferrobasalts (0.70–1.26 wt.%) is lower than that of the majority of continental ferrobasalts (Figure 5(c)). In addition, the Chagangnuoer ferrobasalts have arc signatures of negative Nb, Ta, and Ti anomalies and feature near-flat heavy rare earth elements (Figure 7(a) and 7(b)). The Carboniferous subduction and the early Permian post-collision-related magmatism have been widely discovered in the Awulale Mountains (e.g. Chen *et al.* 2004a, 2004b; Zhu *et al.* 2006a, 2006b, 2009; Li *et al.* 2012b; Yang *et al.* 2012; Yan *et al.* 2013), especially in the Chagangnuoer and adjacent areas. For example Zhang *et al.* (2012a) proposed that the ca. 320 Ma diorite and granitic dikes from the Zhibo area were formed in a continental arc-setting, whereas a ca. 295 Ma granite dike was formed in a post-collision setting. Zhang *et al.* (2014b) suggested that the 350–310 Ma volcanic rocks and related granitoids from the Zhibo and Chagangnuoer areas are chemically similar to arc-related series. Jiang *et al.* (2014) 2014) argued that a ca. 330 Ma andesite in the Zhibo area was formed during slab subduction. Duan *et al.* (2014) proposed that a dacite (ca. 316 Ma) and K-feldspar granite (ca. 297 Ma) in Dunde were formed in subduction and post-collision settings, respectively. Based on the overall
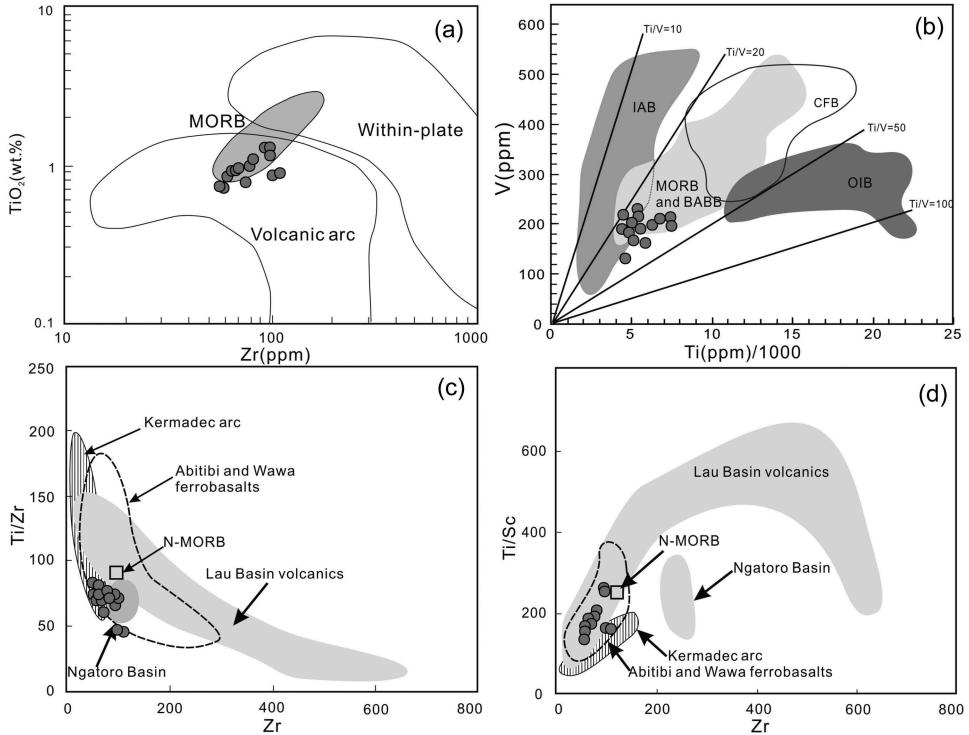
Figure 11.   Tectonic discrimination diagrams of the Chagangnuoer ferrobasalts. (a) TiO_2 *versus* Zr (Pearce 1982); (b) V *versus* Ti/1000 (Shervais 1982); (c) Ti/Zr *versus* Zr (Kerrich *et al.* 2008); and (d) Ti/Sc *versus* Zr (Kerrich *et al.* 2008). Data for the Lau Basin and Abitibi and Wawa volcanic rocks are from Pearce *et al.* (1994) and Kerrich *et al.* (2008), respectively. The Kermadec and Ngatoro fields from Gamble *et al.* (1994) (BABB, back-arc basin basalt; IAB, island arc basalt; CFB, continental flood basalt; OIB, ocean island basalt; N-MORB, normal MORB).

evidence, we suggest that the amalgamation between the Tarim and the YCTP had not occurred during the Devonian–early Carboniferous, and the Chagangnuoer ferrobasalts were formed in a subduction-related setting rather than in a mantle plume or in a continental rift setting.

In the TiO_2 *versus* Zr tectonic discrimination diagram (Figure 11(a)), the Chagangnuoer ferrobasalt data points plot mainly near the boundary between the MORB and arc-volcanic fields. The crystal/liquid partition coefficient for V is predominantly controlled by the oxygen fugacity, whereas that of Ti is not affected (Shervais 1982). Thus, the Ti *versus* V diagram may discriminate the various tectonic settings of volcanic rocks (Shervais 1982). The Chagangnuoer ferrobasalts have Ti/V values varying from 18 to 36 that are plotted mostly in the lower left corner of the MORB-back-arc basin basalt (BABB) field (some samples extend into the island arc basalt (IAB) field) in a Ti/1000 *versus* V diagram (Figure 11(b)). Their geochemical affinity to both MORB- and arc-like rocks might be genetically related to their back-arc basin setting (e.g. Pearce 1982; Taylor and Martinez 2003; Farahat 2010; Baziotis and Mposkos 2011; Zhang *et al.* 2013b). Woodhead *et al.* (1993) and Gamble *et al.* (1994) suggested that the Zr *versus* Ti/Zr and Zr *versus* Ti/Sc

discrimination diagrams can be used to effectively discriminate back-arc basins basalts from arc basalts, due to the back-arc rocks being generally plotted between the MORB and OIB fields and tending to be less hydrous with subdued HFSE/REE fractionations (Kerrich *et al.* 2008). Using these diagrams, Kerrich *et al.* (2008) suggested that the Abitibi and Wawa ferrobasalts were formed in a back-arc environment. In both the Zr *versus* Ti/Zr and Zr *versus* Ti/Sc discrimination diagrams, the Chagangnuoer ferrobasalts plot in the same area as those of the Abitibi and Wawa ferrobasalts (Figure 11(c) and 11(d)), indicating that the Chagangnuoer ferrobasalts could have been formed in a back-arc basin. In addition, a back-arc basin spreading centre produces an extensional environment that facilitates the emplacement of high-density ferrobasalts, and this hypothesis is supported by the Chagangnuoer ferrobasalts having similar formation pressure to that of iron-rich mafic rocks formed in a back-arc basin, for example Abitibi and Wawa and the Zhongtiao Mountains (Figure 10(b)). Coeval arc-related rocks (ca. 314 Ma) have been found in the Laerdundaban area (Zhu *et al.* 2005, 2009), which is located on the northern slope of the Nalati Mountains (Figure 1(b)). We infer that the Nalati Mountains and Awulale Mountains may have constituted a Late Carboniferous arc–back-arc system in
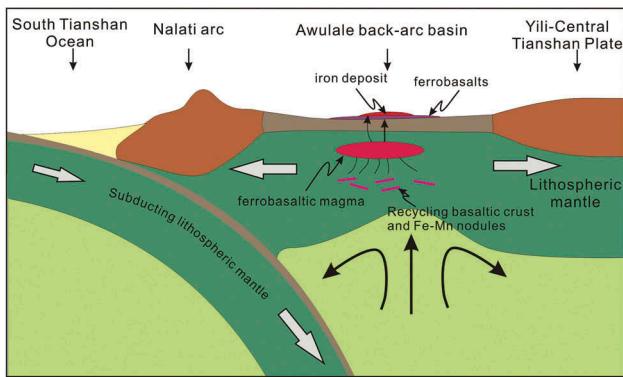
Figure 12. Schematic diagram illustrating the tectonic setting for the generation of the late Carboniferous Chagangnuoer ferrobasalts and iron deposit in western Tianshan.

western Tianshan. The existence of a Late Carboniferous back-arc basin in the Awulale Mountains further supports the proposal that the collision between the Tarim and YCTP had not occurred until ca. 314 Ma.

As a result, we propose a modified Late Carboniferous western Tianshan tectonic model for the Chagangnuoer ferrobasalt petrogenesis (Figure 12). By ca. 314 Ma, an arc–back-arc system was formed in western Tianshan. The lithospheric mantle under the back-arc basin may have been inhomogeneous due to the incorporation of recycling basaltic crust and subducted Fe–Mn nodules into the overlying mantle wedge. Partial melting of such a metasomatized source may have formed the iron-rich magma that ascended and eventually formed the Chagangnuoer ferrobasalts.

5.3. Metallogenesis implications for the Chagangnuoer iron deposit

The Chagangnuoer iron deposit is a magmatic type according to the classification scheme proposed by Dill (2010), based on previous geological and ore observations (Feng *et al.* 2010; Wang *et al.* 2011; Zhang *et al.* 2014b). Ore textures and mineral assemblages reveal that the Chagangnuoer iron deposit was formed through an earlier magmatic period with a later hydrothermal replacement (skarnization) period (Feng *et al.* 2010; Wang *et al.* 2011; Hong *et al.* 2012a, 2012b; Zhang *et al.* 2014b). There are abundant massive and brecciated ores and various conglomerates cemented by ores, indicating that the deposit could be a product of crystallization of iron oxide melts. Last but not least, the $\delta^{18}O$ values of magnetite from the Chagangnuoer iron deposit range from +1.6‰ to +3.3‰ (Feng *et al.* 2010), which is consistent with those of the magnetite from the El Laco deposit in Chile (2.3–4.2‰) (Nyström *et al.* 2008) and the Grängesberg deposit in Sweden (–0.4‰ to +3.7‰) (Jonsson *et al.* 2013). Both the El Laco and Grängesberg deposits have been considered as Kiruna-type iron

deposits, which are the crystallization products of iron oxide melts (Frietsch 1978; Nystroem and Henriquez 1994; Sillitoe and Burrows 2002; Naslund *et al.* 2002; Nyström *et al.* 2008; Jonsson *et al.* 2013). It is noteworthy that magnetite with $\delta^{18}O$ values over 0.9‰ has been proposed as having directly precipitated from magmatic melts at high temperature (Jonsson *et al.* 2013). The relative high $\delta^{18}O$ values of the economic magnetite at Chagangnuoer give further evidence of its magmatic origin. However, the exact metallogenic model of the Kiruna-type iron deposits is still not well constrained (e.g. Naslund *et al.* 2002; Nyström *et al.* 2008; Chen *et al.* 2010; Hou *et al.* 2011).

Feng *et al.* (2010) and Zhang *et al.* (2014b) proposed that the major magmatic iron oxide melts formed the massive and the conglomerates cemented by ores, the secondary hydrothermal fluids formed the miarolitic structure and vein network. These authors also regarded the underlying andesite as the source of iron, because the andesite has similar trace element (e.g. REE) distribution patterns and Pb isotopic compositions with the magnetite (Feng *et al.* 2010; Zhang *et al.* 2014b). Our studies on the ferrobasalts in the Chagangnuoer iron deposit suggest that the parental magma for the ferrobasalts was the most probable source for the iron oxide melts. Despite the presence of minor metallogenic uncertainties, there are some strong supports for our proposal. First, the textures of the major ores (predominately massive ore or conglomerates cemented by ore) are characterized by their magmatic origin as previously documented. Second, the REE and other trace element distribution patterns of the major economic ore, namely the magnetite (Feng *et al.* 2010), are similar to those of the ferrobasalts (Figure 7(b)). Third, previous experimental studies have documented that iron oxide melts can be generated by immiscibility of silicate melts (Philpotts 1967, 1982), which have been used for interpreting the origin of the Fe–Ti–(V) deposits (e.g. Wang and Zhou 2013) and Kiruna-type deposits (Naslund *et al.* 2002; Harlov *et al.* 2002; Chen *et al.* 2010; Chai *et al.* 2014). Melt immiscibility may be related to the increasing P in the magmas (Charlier and Grove 2012). Apatite in the Chagangnuoer iron deposits occurs only as a minute accessory phase and has no spatial association with the iron oxide mineralization (Zhang *et al.* 2014d). However, Lledó (2005) proposed that due to the strong melt polymerization characteristics of the final crystallization stages, even P_2O_5-poor magmas can generate immiscible iron oxide melts. More importantly, the product that formed by melt immiscibility is prevalently composed of two end-members with contrasting chemical compositions, including a low-Si, iron-rich end-member overlying a coeval Si-rich end-member. The coeval felsic rocks (ca. 313 Ma; author's unpublished data) have been recognized in the Chagangnuoer area. Therefore, we conclude that the melt immiscibility of the

ferrobasaltic magma may be applicable to the metallogeny of the Chagangnuoer iron deposit.

6. Conclusions

The ferrobasalts at Chagangnuoer in the Awulale Mountains, western Tianshan, are characterized by high contents of $Fe_2O_3^T$ and MnO, and low TiO_2 contents. Petrological and geochemical data indicate that the ferrobasalts may have been generated from partial melting of a subducted modified lithospheric mantle source. In addition, incorporation of subducted Fe–Mn nodules into the mantle wedge may have played a critical role in forming the iron and Mn enrichments in the Chagangnuoer ferrobasalts. Moreover, the ferrobasaltic magma that formed the ferrobasalts may have been a possible iron source for the Chagangnuoer iron deposit.

References

Allen, M., Windley, B., and Zhang, C., 1993, Palaeozoic collisional tectonics and magmatism of the Chinese Tien Shan, central Asia: Tectonophysics, v. 220, p. 89–115. doi:10.1016/0040-1951(93)90225-9

Ayers, J., 1998, Trace element modeling of aqueous fluid–peridotite interaction in the mantle wedge of subduction zones: Contributions to Mineralogy and Petrology, v. 132, p. 390–404. doi:10.1007/s004100050431

Baker, J.A., and Krogh Jensen, K., 2004, Coupled ^{186}Os–^{187}Os enrichments in the Earth's mantle-core-mantle interaction or recycling of ferromanganese crusts and nodules? Earth and Planetary Science Letters, v. 220, p. 277–286. doi:10.1016/S0012-821X(04)00059-7

Baziotis, I., and Mposkos, E., 2011, Origin of metabasites from upper tectonic unit of the Lavrion area (SE Attica, Greece): Geochemical implications for dual origin with distinct provenance of blueschist and greenschist's protoliths: Lithos, v. 126, p. 161–173. doi:10.1016/j.lithos.2011.07.014

Belousova, E., Griffin, W.L., O'Reilly, S.Y., and Fisher, N., 2002, Igneous zircon: Trace element composition as an indicator of source rock type: Contributions to Mineralogy and Petrology, v. 143, p. 602–622. doi:10.1007/s00410-002-0364-7

Berry, A.J., Yaxley, G.M., Hanger, B.J., Woodland, A.B., de Jonge, M.D., Howard, D.L., Paterson, D., and Kamenetsky, V.S., 2013, Quantitative mapping of the oxidative effects of mantle metasomatism: Geology, v. 41, p. 683–686. doi:10.1130/G34119.1

Black, L.P., Kamo, S.L., Allen, C.M., Davis, D.W., Aleinikoff, J. N., Valley, J.W., Mundil, R., Campbell, I.H., Korsch, R.J., Williams, I.S., and Foudoulis, C., 2004, Improved ^{206}Pb/^{238}U microprobe geochronology by the monitoring of a trace element related matrix effect; SHRIMP, ID-TIMS, ELA-ICP-MS and oxygen isotope documentation for a series of zircon standards: Chemical Geology, v. 205, no. 1–2, p. 115–140. doi:10.1016/j.chemgeo.2004.01.003

Botcharnikov, R.E., Almeev, R.R., Koepke, J., and Holtz, F., 2008, Phase Relations and Liquid Lines of Descent in Hydrous Ferrobasalt – Implications for the Skaergaard Intrusion and Columbia River flood basalts: Journal of Petrology, v. 49, p. 1687–1727. doi:10.1093/petrology/egn043

Brenan, J., Shaw, H., Ryerson, F., and Phinney, D., 1995, Mineral-aqueous fluid partitioning of trace elements at 900° C and 2.0 GPa: Constraints on the trace element chemistry of mantle and deep crustal fluids: Geochimica Et Cosmochimica Acta, v. 59, p. 3331–3350. doi:10.1016/0016-7037(95)00215-L

Brooks, C.K., Larsen, L.M., and Nielsen, T.F.D., 1991, Importance of iron-rich tholeiitic magmas at divergent plate margins: A reappraisal: Geology, v. 19, p. 269–272. doi:10.1130/0091-7613(1991)019<0269:IOIRTM>2.3.CO;2

Cawood, P.A., Kröner, A., Collins, W.J., Kusky, T.M., Mooney, W.D., and Windley, B.F., 2009, Accretionary orogens through Earth history: Geological Society, London, Special Publications, v. 318, p. 1–36. doi:10.1144/SP318.1

Chai, F., Yang, F., Liu, F., Santosh, M., Geng, X., Li, Q., and Liu, G., 2014, The Abagong apatite-rich magnetite deposit in the Chinese Altay Orogenic Belt: A Kiruna-type iron deposit: Ore Geology Reviews, v. 57, p. 482–497. doi:10.1016/j.oregeorev.2013.07.002

Charlier, B., and Grove, T.L., 2012, Experiments on liquid immiscibility along tholeiitic liquid lines of descent: Contributions to Mineralogy and Petrology, v. 164, p. 27–44. doi:10.1007/s00410-012-0723-y

Charvet, J., Shu, L.S., and Laurent-Charvet, S., 2007, Paleozoic structural and geodynamic evolution of eastern Tianshan (NW China): Welding of the Tarim and Junggar plates: Episodes, v. 30, p. 162–186.

Che, Z.C., Liu, L., Liu, H.F., and Luo, J.H., 1996, Review on the ancient Yili rift, Xinjiang, China: Acta Petrologica Sinica, v. 12, p. 478–490. [In Chinese with English abstract.]

Chen, C.M., Lu, H.F., Jia, D., Cai, D.S., and Wu, S.M., 1999, Closing history of the southern Tianshan oceanic basin, western China: An oblique collisional orogeny: Tectonophysics, v. 302, p. 23–40. doi:10.1016/S0040-1951(98)00273-X

Chen, H.Y., Clark, A.H., and Kyser, T.K., 2010, The Marcona magnetite deposit, Ica, South-Central Peru: A product of hydrous, iron oxide-rich melts?: Economic Geology, v. 105, p. 1441–1456. doi:10.2113/econgeo.105.8.1441

Chen, Y.J., Bao, J.X., Zhang, Z.J., Liu, Y.L., Chen, H.Y., Cai, W. J., and Helmstaedt, H., 2004a, Tectonic setting and element geochemistry of the Aikendaban formation volcanic rocks in west Tianshan: J Mineral Petrol, v. 24, p. 36–45. [In Chinese with English abstract.]

Chen, Y.J., Liu, Y.L., Bao, J.X., Zhang, Z.J., Chen, H.Y., Cai, W. J., and Helmstaedt, H., 2004b, Isotopic dating for the

volcanic rocks of the Aikendaban formation in West Tianshan, China and its tectonic implication: J Mineral Petrol, v. 24, p. 52–55. [In Chinese with English abstract.]

Class, C., Miller, D.M., Goldstein, S.L., and Langmuir, C.H., 2000, Distinguishing melt and fluid subduction components in Umnak Volcanics, Aleutian Arc: Geochemistry, Geophysics, Geosystems, v. 1, p. 1004. doi:10.1029/1999GC000010

Dill, H.G., 2010, The "chessboard" classification scheme of mineral deposits: Mineralogy and geology from aluminum to zirconium: Earth Science Reviews, v. 100, p. 1–420. doi:10.1016/j.earscirev.2009.10.011

Ding, X., Hu, Y.H., Zhang, H., Li, C.Y., Ling, M.X., and Sun, W. D., 2013, Major Nb/Ta fractionation recorded in garnet amphibolite facies metagabbro: The Journal of Geology, v. 121, p. 255–274. doi:10.1086/669978

Ding, X., Lundstrom, C., Huang, F., Li, J., Zhang, Z.M., Sun, X.M., Liang, J.L., and Sun, W.D., 2009, Natural and experimental constraints on formation of the continental crust based on niobium–tantalum fractionation: International Geology Review, v. 51, p. 473–501. doi:10.1080/00206810902759749

Duan, S., Zhang, Z., Jiang, Z., Zhao, J., Zhang, Y., Li, F., and Tian, J., 2014, Geology, geochemistry, and geochronology of the Dunde iron–zinc ore deposit in western Tianshan, China: Ore Geology Reviews, v. 57, p. 441–461. doi:10.1016/j.oregeorev.2013.08.019

Evans, K., Elburg, M., and Kamenetsky, V., 2012, Oxidation state of subarc mantle: Geology, v. 40, p. 783–786. doi:10.1130/G33037.1

Farahat, E., 2010, Neoproterozoic arc-back-arc system in the Central Eastern Desert of Egypt: Evidence from supra–subduction zone ophiolites: Lithos, v. 120, p. 293–308. doi:10.1016/j.lithos.2010.08.017

Faure, G., and Mensing, T.M., 2005, Isotopes: Principles and applications: Hoboken, NJ, Wiley .

Feng, J., Shi, F., Wang, B., Hu, J., Wang, J., and Tian, J., 2010, The syn-genetic volcanogenic iron ore deposits in Awulale Metallogenetic Belt, Western Tianshan Mountains: Beijing, Geological Publishing House. [In Chinese.]

Fisk, M.R., 1986, Mid- ocean ridge basalts from the Galápagos spreading center: Direct probes of magma chambers: Geology, v. 14, p. 204–207. doi:10.1130/0091-7613(1986)14<204:MRBFTG>2.0.CO;2

Francis, D., Ludden, J., Johnstone, R., and Davis, W., 1999, Picrite evidence for more Fe in Archean mantle reservoirs: Earth and Planetary Science Letters, v. 167, p. 197–213. doi:10.1016/S0012-821X(99)00032-1

Frietsch, R., 1978, On the magmatic origin of iron ores of the Kiruna type: Economic Geology, v. 73, p. 478–485. doi:10.2113/gsecongeo.73.4.478

Gamble, J., Wright, I., Woodhead, J., and McCulloch, M., 1994, Arc and back–arc geochemistry in the southern Kermadec arc–Ngatoro Basin and offshore Taupo Volcanic Zone, SW Pacific: Geological Society, London, Special Publications, v. 81, p. 193–212. doi:10.1144/GSL.SP.1994.081.01.11

Gao, J., Long, L.L., Klemd, R., Qian, Q., Liu, D.Y., Xiong, X. M., Su, W., Liu, W., Wang, Y.T., and Yang, F.Q., 2009, Tectonic evolution of the South Tianshan orogen and adjacent regions, NW China: Geochemical and age constraints of granitoid rocks: International Journal of Earth Sciences, v. 98, p. 1221–1238. doi:10.1007/s00531-008-0370-8

Genç, Ş., and Tüysüz, O., 2010, Tectonic setting of the Jurassic bimodal magmatism in the Sakarya Zone (Central and Western Pontides), Northern Turkey: A geochemical and

isotopic approach: Lithos, v. 118, p. 95–111. doi:10.1016/j.lithos.2010.03.017

Gibson, S.A., 2002, Major element heterogeneity in Archean to Recent mantle plume starting – Heads: Earth and Planetary Science Letters, v. 195, p. 59–74. doi:10.1016/S0012-821X(01)00566-0

Gibson, S.A., Thompson, R.N., and Dickin, A.P., 2000, Ferropicrites: Geochemical evidence for Fe-rich streaks in upwelling mantle plumes: Earth and Planetary Science Letters, v. 174, p. 355–374. doi:10.1016/S0012-821X(99)00274-5

Han, B.-F., Guo, Z.-J., Zhang, Z.-C., Zhang, L., Chen, J.-F., and Song, B., 2010, Age, geochemistry, and tectonic implications of a late Paleozoic stitching pluton in the North Tian Shan suture zone, western China: Geological Society of America Bulletin, v. 122, p. 627–640. doi:10.1130/B26491.1

Harlov, D.E., Andersson, U.B., Förster, H.-J., Nyström, J.O., Dulski, P., and Broman, C., 2002, Apatite-monazite relations in the Kiirunavaara magnetite-apatite ore, northern Sweden: Chemical Geology, v. 191, p. 47–72. doi:10.1016/S0009-2541(02)00148-1

Hart, S., Gerlach, D., and White, W., 1986, A possible new Sr–Nd–Pb mantle array and consequences for mantle mixing: Geochimica Et Cosmochimica Acta, v. 50, p. 1551–1557. doi:10.1016/0016-7037(86)90329-7

Hart, S., Hauri, E., Oschmann, L., and Whitehead, J., 1992, Mantle plumes and entrainment: Isotopic evidence: Science, v. 256, p. 517–520. doi:10.1126/science.256.5056.517

Heinhorst, J., Lehmann, B., Ermolov, P., Serykh, V., and Zhurutin, S., 2000, Paleozoic crustal growth and metallogeny of Central Asia: Evidence from magmatic–hydrothermal ore systems of Central Kazakhstan: Tectonophysics, v. 328, p. 69–87. doi:10.1016/S0040-1951(00)00178-5

Hirose, K., and Kushiro, I., 1993, Partial melting of dry peridotites at high pressures: Determination of compositions of melts segregated from peridotite using aggregates of diamond: Earth and Planetary Science Letters, v. 114, p. 477–489. doi:10.1016/0012-821X(93)90077-M

Hong, W., Zhang, Z.H., Jiang, Z.S., Li, F.M., and Liu, X.Z., 2012a, Magnetite and garnet trace element characteristics from the Chagangnuoer iron deposit in the western Tianshan Mountains, Xinjiang, NW China: Constrain for ore genesis: Acta Petrologica Sinica, v. 28, p. 2089–2102. [In Chinese with English abstract.]

Hong, W., Zhang, Z.H., Li, H.Q., Li, F.M., and Liu, X.Z., 2012b, Metallogenic epoch of Chagangnuoer iron deposit in western Tianshan Mountains, Xinjiang: Information from garnet Sm–Nd isochron age: Mineral Deposits, v. 31, p. 1067–1074. [In Chinese with English abstract.]

Hoskin, P., and Black, L., 2000, Metamorphic zircon formation by solid-state recrystallization of protolith igneous zircon: Journal of Metamorphic Geology, v. 18, p. 423–439. doi:10.1046/j.1525-1314.2000.00266.x

Hou, T., Zhang, Z., and Kusky, T., 2011, Gushan magnetite–apatite deposit in the Ningwu basin, Lower Yangtze River Valley, SE China: Hydrothermal or Kiruna-type? Ore Geology Reviews, v. 43, p. 333–346. doi:10.1016/j.oregeorev.2011.09.014

Hou, T., Zhang, Z.C., Pirajno, F., Santosh, M., Encarnacion, J., Liu, J.L., Zhao, Z.D., and Zhang, L.J., 2014, Geology, tectonic settings and iron ore metallogenesis associated with submarine volcanism in China: An overview: Ore Geology Reviews, v. 57, p. 498–517. doi:10.1016/j.oregeorev.2013.08.007

Ichiyama, Y., and Ishiwatari, A., 2005, HFSE-rich picritic rocks from the Mino accretionary complex, southwestern Japan: Contributions to Mineralogy and Petrology, v. 149, p. 373–387. doi:10.1007/s00410-005-0659-6

Ichiyama, Y., Ishiwatari, A., Hirahara, Y., and Shuto, K., 2006, Geochemical and isotopic constraints on the genesis of the Permian ferropicritic rocks from the Mino–Tamba belt, SW Japan: Lithos, v. 89, p. 47–65. doi:10.1016/j.lithos.2005.09.006

Jang, Z., Zhang, Z., Hou, K., Hong, W., Wang, Z., Li, F., and Tian, J., 2012, Geochemistry and zircon U–Pb ages of volcanic rocks from the Chagangnuoer and Zhibo iron deposits, western Tianshan, and their geological significance: Acta Petrologica Sinica, v. 28, p. 2074–2088. [In Chinese with English abstract.]

Jensen, L.S., 1976, A new cation plot for classifying subalkalic volcanic rocks: Ontario Division of Mines, Miscellaneous Paper 66, 21 p.

Jiang, Y.-H., Jiang, S.-Y., Dai, B.-Z., Liao, S.-Y., Zhao, K.-D., and Ling, H.-F., 2009, Middle to late Jurassic felsic and mafic magmatism in southern Hunan province, southeast China: Implications for a continental arc to rifting: Lithos, v. 107, p. 185–204. doi:10.1016/j.lithos.2008.10.006

Jiang, Z., Zhang, Z., Wang, Z., Duan, S., Li, F., and Tian, J., 2014, Geology, geochemistry, and geochronology of the Zhibo iron deposit in the Western Tianshan, NW China: Constraints on metallogenesis and tectonic setting: Ore Geology Reviews, v. 57, p. 406–424. doi:10.1016/j.oregeorev.2013.09.016

Jonsson, E., Troll, V.R., Högdahl, K., Harris, C., Weis, F., Nilsson, K.P., and Skelton, A., 2013, Magmatic origin of giant 'Kiruna-type' apatite-iron-oxide ores in Central Sweden: Scientific Reports, v. 3, p. 1644. doi:10.1038/srep01644

Kawamoto, T., and Holloway, J.R., 1997, Melting temperature and partial melt chemistry of H_2O-saturated mantle peridotite to 11 gigapascals: Science, v. 276, p. 240–243. doi:10.1126/science.276.5310.240

Kelley, K.A., and Cottrell, E., 2009, Water and the oxidation state of subduction zone magmas: Science, v. 325, p. 605–607. doi:10.1126/science.1174156

Kelley, K.A., and Cottrell, E., 2012, The influence of magmatic differentiation on the oxidation state of Fe in a basaltic arc magma: Earth and Planetary Science Letters, v. 329–330, p. 109–121. doi:10.1016/j.epsl.2012.02.010

Kerrich, R., Polat, A., Wyman, D., and Hollings, P., 1999, Trace element systematics of Mg-, to Fe- tholeiitic basalt suites of the Superior Province: Implications for Archean mantle reservoirs and greenstone belt genesis: Lithos, v. 46, p. 163–187. doi:10.1016/S0024-4937(98)00059-0

Kerrich, R., Polat, A., and Xie, Q.L., 2008, Geochemical systematics of 2.7 Ga Kinojevis Group (Abitibi), and Manitouwadge and Winston Lake (Wawa) Fe-rich basalt–rhyolite associations: Backarc rift oceanic crust? Lithos, v. 101, p. 1–23. doi:10.1016/j.lithos.2007.07.009

Kogiso, T., Hirose, K., and Takahashi, E., 1998, Melting experiments on homogeneous mixtures of peridotite and basalt: Application to the genesis of ocean island basalts: Earth and Planetary Science Letters, v. 162, p. 45–61. doi:10.1016/S0012-821X(98)00156-3

Lassiter, J.C., and DePaolo, D.J., 1997, Plume/lithosphere interaction in the generation of continental and oceanic flood basalts: Chemical and isotopic constraints, *in* Mahoney, J.J., and Coffin, M.F., eds., Large igneous provinces: Continental, oceanic and planetary flood volcanism:

American Geophysical Union, Geophysical Monograph 100, p. 335–355.

Leroex, A.P., and Dick, H.J.B., 1981, Petrography and geochemistry of basaltic rocks from the Conrad Fracture Zone on the America – Antarctica Ridge: Earth and Planetary Science Letters, v. 54, p. 117–138. doi:10.1016/0012-821X(81)90073-X

Leroex, A.P., Dick, H.J.B., Reid, A.M., and Erlank, A.J., 1982, Ferrobasalts from the Spiess Ridge segment of the Southwest Indian Ridge: Earth and Planetary Science Letters, v. 60, p. 437–451. doi:10.1016/0012-821X(82)90079-6

Leybourne, M.I., van Wagoner, N., and Ayres, L.D., 1999, Partial melting of a refractory subducted slab in a Paleoproterozoic island arc: Implications for global chemical cycles: Geology, v. 27, p. 731–734. doi:10.1130/0091-7613(1999)027<0731:PMOARS>2.3.CO;2

Li, C.-Y., Zhang, H., Wang, F.-Y., Liu, J.-Q., Sun, Y.-L., Hao, X.-L., Li, Y.-L., and Sun, W.D., 2012a, The formation of the Dabaoshan porphyry molybdenum deposit induced by slab rollback: Lithos, v. 150, p. 101–110. doi:10.1016/j.lithos.2012.04.001

Li, J.-L., Gao, J., John, T., Klemd, R., and Su, W., 2013, Fluid-mediated metal transport in subduction zones and its link to arc-related giant ore deposits: Constraints from a sulfide-bearing HP vein in lawsonite eclogite (Tianshan, China): Geochimica Et Cosmochimica Acta, v. 120, p. 326–362. doi:10.1016/j.gca.2013.06.023

Li, N.-B., Niu, H.-C., Bao, Z.-W., Shan, Q., Yang, W.-B., Jiang, Y.-H., and Zeng, L.-J., 2014, Geochronology and geochemistry of the Paleoproterozoic Fe-rich mafic sills from the Zhongtiao Mountains: Petrogenesis and tectonic implications: Precambrian Research, v. 255, Part 2, p. 668–684. doi:10.1016/j.precamres.2014.08.019

Li, N.B., Shan, Q., Zhang, Y.P., Luo, Y., Yang, W.B., Jiang, Y.H., and Yu, X.Y., 2012b, Study on the A-type rhyolite porphyries from the Awulale area, western Tianshan: Geotectonica Et Metallogenia, v. 36, p. 624–633. [In Chinese with English abstract.]

Li, X., Qi, C., Liu, Y., Liang, X., Tu, X., Xie, L., and Yang, Y., 2005, Petrogenesis of the Neoproterozoic bimodal volcanic rocks along the western margin of the Yangtze Block: New constraints from Hf isotopes and Fe/Mn ratios: Chinese Science Bulletin, v. 50, p. 2481–2486. doi:10.1360/982005-287

Li, X.-H., 1997, Geochemistry of the Longsheng Ophiolite from the southern margin of Yangtze Craton, SE China: Geochemical Journal Japan, v. 31, p. 323–337. doi:10.2343/geochemj.31.323

Liang, H.-Y., Campbell, I.H., Allen, C., Sun, W.-D., Liu, C.-Q., Yu, H.-X., Xie, Y.-W., and Zhang, Y.-Q., 2006, Zircon Ce^{4+}/Ce^{3+} ratios and ages for Yulong ore-bearing porphyries in eastern Tibet: Mineralium Deposita, v. 41, p. 152–159. doi:10.1007/s00126-005-0047-1

Liang, J.L., Ding, X., Sun, X.M., Zhang, Z.M., Zhang, H., and Sun, W.D., 2009, Nb/Ta fractionation observed in eclogites from the Chinese Continental Scientific Drilling Project: Chemical Geology, v. 268, p. 27–40. doi:10.1016/j.chemgeo.2009.07.006

Liang, X.R., Wei, G.J., Li, X.H., and Liu, Y., 2003, Precise measurement of $^{143}Nd/^{144}Nd$ and Sm/Nd ratios using multiple-collectors inductively coupled plasma–mass spectrometer (MC – ICPMS): Geochimica, v. 32, p. 91–96. [In Chinese with English abstract.]

Ling, M.-X., Liu, Y.-L., Williams, I.S., Teng, F.-Z., Yang, X.-Y., Ding, X., Wei, G.-J., Xie, L.-H., Deng, W.-F., and Sun, W.-D., 2013, Formation of the world's largest REE deposit

through protracted fluxing of carbonatite by subduction-derived fluids: Scientific Reports, v. 3, p. 1–8. doi:10.1038/srep01776

Lledó, L.H., 2005, Experimental studies on the origin of iron deposits and mineralization of Sierra La Bandera, Chile [Unpublished Ph.D. thesis]: Binghamton, NY, State University of New York, 200 p.

Long, L.L., Gao, J., Klemd, R., Beier, C., Qian, Q., Zhang, X., Wang, J.B., and Jiang, T., 2011, Geochemical and geochronological studies of granitoid rocks from the Western Tianshan Orogen: Implications for continental growth in the southwestern Central Asian Orogenic Belt: Lithos, v. 126, p. 321–340. doi:10.1016/j.lithos.2011.07.015

Ludwig, K., 2008, Isoplot 3.6; a geochronology toolkit for Microsoft Excel: Berkeley, California, Geochronology Center, 77 p.

Marschall, H.R., and Schumacher, J.C., 2012, Arc magmas sourced from mélange diapirs in subduction zones: Nature Geoscience, v. 5, p. 862–867. doi:10.1038/ngeo1634

Mayer, B., Jung, S., Romer, R., Stracke, A., Haase, K., and Garbe-Schönberg, C.-D., 2013, Petrogenesis of Tertiary Hornblende- bearing Lavas in the Rhön, Germany: Journal of Petrology, v. 54, p. 2095–2123. doi:10.1093/petrology/egt042

Naslund, H., Henríquez, F., Nyström, J., Vivallo, W., and Dobbs, F., 2002, Magmatic iron ores and associated mineralization: Examples from the Chilean High Andes and Coastal Cordillera: Hydrothermal iron oxide copper-gold and related deposits: A Global Perspective, v. 2, p. 207–226.

Nystroem, J.O., and Henriquez, F., 1994, Magmatic features of iron ores of the Kiruna type in Chile and Sweden; ore textures and magnetite geochemistry: Economic Geology, v. 89, p. 820–839. doi:10.2113/gsecongeo.89.4.820

Nyström, J.O., Billström, K., Henríquez, F., Fallick, A.E., and Naslund, H.R., 2008, Oxygen isotope composition of magnetite in iron ores of the Kiruna type in Chile and Sweden: Gff, v. 130, p. 177–188. doi:10.1080/11035890809452771

Pearce, J.A., 1982, Trace element characteristics of lavas from destructive plate boundaries, *in* Thorpe, R.S., ed., Andesites: New York, Wiley, p. 525–548.

Pearce, J.A., Ernewein, M., Bloomer, S.H., Parson, L.M., Murton, B.J., and Johnson, L.E., 1994, Geochemistry of Lau Basin volcanic rocks: Influence of ridge segmentation and arc proximity: Geological Society, London, Special Publications, v. 81, p. 53–75. doi:10.1144/GSL.SP.1994.081.01.04

Peng, P., Zhai, M.-G., Guo, J.-H., Kusky, T., and Zhao, T.-P., 2007, Nature of mantle source contributions and crystal differentiation in the petrogenesis of the 1.78 Ga mafic dykes in the central North China Craton: Gondwana Research, v. 12, p. 29–46. doi:10.1016/j.gr.2006.10.022

Peng, T.P., Wilde, S.A., Fan, W.M., Peng, B.X., and Mao, Y.S., 2013, Mesoproterozoic high Fe–Ti mafic magmatism in western Shandong, North China Craton: Petrogenesis and implications for the final breakup of the Columbia supercontinent: Precambrian Research, v. 235, p. 190–207. doi:10.1016/j.precamres.2013.06.013

Philpotts, A., 1967, Origin of certain iron-titanium oxide and apatite rocks: Economic Geology, v. 62, p. 303–315. doi:10.2113/gsecongeo.62.3.303

Philpotts, A., 1982, Compositions of immiscible liquids in volcanic rocks: Contributions to Mineralogy and Petrology, v. 80, p. 201–218. doi:10.1007/BF00371350

Rudnick, R.L., and Fountain, D.M., 1995, Nature and composition of the continental crust: A lower crustal perspective:

Reviews of Geophysics, v. 33, p. 267–309. doi:10.1029/95RG01302

Said, N., and Kerrich, R., 2010, Elemental and Nd-isotope systematics of the Upper Basalt Unit, 2.7 Ga Kambalda Sequence: Quantitative modeling of progressive crustal contamination of plume asthenosphere: Chemical Geology, v. 273, p. 193–211.

Salters, V.J.M., and Stracke, A., 2004, Composition of the depleted mantle: Geochemistry, Geophysics, Geosystems, v. 5, p. Q05B07. doi:10.1029/2003GC000597

Şengör, A.M.C., Natal'in, B.A., and Burtman, V.S., 1993, Evolution of the Altaid tectonic collage and Palaeozoic crustal growth in Eurasia: Nature, v. 364, p. 299–307. doi:10.1038/364299a0

Shan, Q., Zhang, B., Luo, Y., Zhou, C., Yu, X., Zeng, Q., Yang, W., and Niu, H., 2009, Characteristics and trace element geochemistry of pyrite from the Songhu iron deposit, Nilek County, Xinjiang, China: Acta Petrologica Sinica, v. 25, p. 1456–1464. [In Chinese with English abstract.]

Shervais, J.W., 1982, Ti–V plots and the petrogenesis of modern and ophiolitic lavas: Earth and Planetary Science Letters, v. 59, p. 101–118. doi:10.1016/0012-821X(82)90120-0

Shu, L.S., Wang, B., Zhu, W.B., Guo, Z.J., Charvet, J., and Zhang, Y., 2011, Timing of initiation of extension in the Tianshan, based on structural, geochemical and geochronological analyses of bimodal volcanism and olistostrome in the Bogda Shan (NW China): International Journal of Earth Sciences, v. 100, p. 1647–1663. doi:10.1007/s00531-010-0575-5

Sillitoe, R.H., and Burrows, D.R., 2002, New field evidence bearing on the origin of the El Laco magnetite deposit, northern Chile: Economic Geology, v. 97, p. 1101–1109.

Sobolev, A.V., Hofmann, A.W., Kuzmin, D.V., Yaxley, G.M., Arndt, N.T., Chung, S.-L., Danyushevsky, L.V., Elliott, T., Frey, F.A., Garcia, M.O., Gurenko, A.A., Kamenetsky, V.S., Kerr, A.C., Krivolutskaya, N.A., Matvienkov, V.V., Nikogosian, I.K., Rocholl, A., Sigurdsson, I.A., Sushchevskaya, N.M., and Teklay, M., 2007, The amount of recycled crust in sources of mantle–derived melts: Science, v. 316, p. 412–417. doi:10.1126/science.1138113

Su, B.-X., Qin, K.-Z., Sakyi, P.A., Li, X.-H., Yang, Y.-H., Sun, H., Tang, D.-M., Liu, P.-P., Xiao, Q.-H., and Malaviarachchi, S.P.K., 2011, U–Pb ages and Hf–O isotopes of zircons from Late Paleozoic mafic–ultramafic units in the southern Central Asian Orogenic Belt: Tectonic implications and evidence for an Early-Permian mantle plume: Gondwana Research, v. 20, p. 516–531. doi:10.1016/j.gr.2010.11.015

Sun, -S.-S., and McDonough, W., 1989, Chemical and isotopic systematics of oceanic basalts: Implications for mantle composition and processes: Geological Society, London, Special Publications, v. 42, p. 313–345. doi:10.1144/GSL.SP.1989.042.01.19

Sun, W.D., Bennett, V.C., and Kamenetsky, V.S., 2004, The mechanism of Re enrichment in arc magmas: Evidence from Lau Basin basaltic glasses and primitive melt inclusions: Earth and Planetary Science Letters, v. 222, p. 101–114.

Sun, W.D., Huang, R.-F., Li, H., Hu, Y.-B., Zhang, C.-C., Sun, S.-J., Zhang, L.-P., Ding, X., Li, C.-Y., Zartman, R.E., and Ling, M.-X., 2015, Porphyry deposits and oxidized magmas: Ore Geology Reviews, v. 65, p. 97–131. doi:10.1016/j.oregeorev.2014.09.004

Sun, W.-D., Liang, H.-Y., Ling, M.-X., Zhan, M.-Z., Ding, X., Zhang, H., Yang, X.-Y., Li, Y.-L., Ireland, T.R., Wei, Q.-R., and Fan, W.-M., 2013, The link between reduced porphyry copper deposits and oxidized magmas: Geochimica Et

Cosmochimica Acta, v. 103, p. 263–275. doi:10.1016/j.gca.2012.10.054

Sun, X.M., Tang, Q., Sun, W.D., Xu, L., Zhai, W., Liang, J.L., Liang, Y.H., Shen, K., Zhang, Z.M., Zhou, B., and Wang, F. Y., 2007, Monazite, iron oxide and barite exsolutions in apatite aggregates from CCSD drillhole eclogites and their geological implications: Geochimica Et Cosmochimica Acta, v. 71, p. 2896–2905. doi:10.1016/j.gca.2007.03.030

Tatsumi, Y., Hamilton, D.L., and Nesbitt, R.W., 1986, Chemical characteristics of fluid phase released from a subducted lithosphere and origin of arc magmas: Evidence from high-pressure experiments and natural rocks: Journal of Volcanology and Geothermal Research, v. 29, p. 293–309. doi:10.1016/0377-0273(86)90049-1

Taylor, B., and Martinez, F., 2003, Back-arc basin basalt systematics: Earth and Planetary Science Letters, v. 210, p. 481–497. doi:10.1016/S0012-821X(03)00167-5

Taylor, S.R., and McLennan, S.M., 1985, The continental crust: Its composition and evolution: Oxford, Blackwell Scientific Publications, 312 p.

Temizel, İ., Arslan, M., Ruffet, G., and Peucat, J.J., 2012, Petrochemistry, geochronology and Sr–Nd isotopic systematics of the Tertiary collisional and post-collisional volcanic rocks from the Ulubey (Ordu) area, eastern Pontide, NE Turkey: Implications for extension-related origin and mantle source characteristics: Lithos, v. 128, p. 126–147.

Trail, D., Watson, E.B., and Tailby, N.D., 2011, The oxidation state of Hadean magmas and implications for early Earth's atmosphere: Nature, v. 480, p. 79–82. doi:10.1038/nature10655

Tu, X., Zhang, H., Deng, W., Ling, M., Liang, H., Liu, Y., and Sun, W., 2011, Application of RESOlution in-situ laser ablation ICP-MS in trace element analyses: Geochimica, v. 40, p. 83–98. [In Chinese with English abstract.]

Wang, B.Y., Hu, X.J., Wang, J.T., Shao, Q.H., Ling, J.L., Gou, N.X., Zhao, Y.F., Xia, Z.D., and Jiang, C.Y., 2011, Geological characteristics and genesis of Chagannur iron deposit in Western Tianshan, Xinjiang: Mineral Deposits, v. 30, p. 385–402. [In Chinese with English abstract.]

Wang, C.Y., and Zhou, M.-F., 2013, New textural and mineralogical constraints on the origin of the Hongge Fe-Ti-V oxide deposit, SW China: Mineralium Deposita, v. 48, p. 787–798. doi:10.1007/s00126-013-0457-4

Wang, J., and Xu, X., 2006, Post-collisional tectonic evolution and metallogenesis in northern Xinjiang, China: Acta Geologica Sinica, v. 80, p. 23–31. [In Chinese with English abstract.]

Wang, Y., Fan, W., Zhang, Y., Guo, F., Zhang, H., and Peng, T., 2004, Geochemical, $^{40}Ar/^{39}Ar$ geochronological and Sr–Nd isotopic constraints on the origin of Paleoproterozoic mafic dikes from the southern Taihang Mountains and implications for the ca. 1800Ma event of the North China Craton: Precambrian Research, v. 135, p. 55–77. doi:10.1016/j.precamres.2004.07.005

Wang, Y., Zhao, G., Cawood, P.A., Fan, W., Peng, T., and Sun, L., 2008, Geochemistry of Paleoproterozoic (~1770Ma) mafic dikes from the Trans-North China Orogen and tectonic implications: Journal of Asian Earth Sciences, v. 33, p. 61–77. doi:10.1016/j.jseaes.2007.10.018

Wang, Z., Wu, J., Lu, X., Liu, C., and Zhang, J., 1990, Polycyclic tectonic evolution and metallogeny of the Tianshan Mountains: Beijing, Science Press, v. 29, p. r37. [In Chinese.]

Wei, G.J., Liang, X.R., Li, X.H., and Liu, Y., 2002, Precise measurement of Sr isotopic composition of liquid and solid base using (LP) MC-ICPMS: Geochimica, v. 31, p. 295–305. [In Chinese with English abstract.]

Windley, B.F., Alexeiev, D., Xiao, W.J., Kroner, A., and Badarch, G., 2007, Tectonic models for accretion of the Central Asian Orogenic Belt: Journal of the Geological Society, v. 164, p. 31–47. doi:10.1144/0016-76492006-022

Woodhead, J., Eggins, S., and Gamble, J., 1993, High field strength and transition element systematics in island arc and back-arc basin basalts: Evidence for multi-phase melt extraction and a depleted mantle wedge: Earth and Planetary Science Letters, v. 114, p. 491–504. doi:10.1016/0012-821X(93)90078-N

Xia, L.-Q., Xia, Z.-C., Xu, X.-Y., Li, X.-M., and Ma, Z.-P., 2008, Relative contributions of crust and mantle to the generation of the Tianshan Carboniferous rift-related basic lavas, northwestern China: Journal of Asian Earth Sciences, v. 31, p. 357–378. doi:10.1016/j.jseaes.2007.07.002

Xia, L.Q., Xia, Z.C., Xu, X.Y., Li, X.M., Ma, Z.P., and Wang, L. S., 2004a, Carboniferous Tianshan igneous megaprovince and mantle plume: Regional Geology of China Z, v. 2, p. 903–910. [In Chinese.]

Xia, L.-Q., Xu, X.-Y., Xia, Z.-C., Li, X.-M., Ma, Z.-P., and Wang, L.-S., 2004b, Petrogenesis of Carboniferous rift-related volcanic rocks in the Tianshan, northwestern China: Geological Society of America Bulletin, v. 116, p. 419–433. doi:10.1130/B25243.1

Xiao, W.J., Huang, B.C., Han, C.M., Sun, S., and Li, J.L., 2010, A review of the western part of the Altaids: A key to understanding the architecture of accretionary orogens: Gondwana Research, v. 18, p. 253–273. doi:10.1016/j.gr.2010.01.007

Xiao, W.J., Windley, B.F., Allen, M.B., and Han, C.M., 2013, Paleozoic multiple accretionary and collisional tectonics of the Chinese Tianshan orogenic collage: Gondwana Research, v. 23, p. 1316–1341. doi:10.1016/j.gr.2012.01.012

Xiao, W.J., Windley, B.F., Huang, B.C., Han, C.M., Yuan, C., Chen, H.L., Sun, M., Sun, S., and Li, J.L., 2009, End-Permian to mid-Triassic termination of the accretionary processes of the southern Altaids: Implications for the geodynamic evolution, Phanerozoic continental growth, and metallogeny of Central Asia: International Journal of Earth Sciences, v. 98, p. 1189–1217. doi:10.1007/s00531-008-0407-z

Xiao, W.J., Zhang, L.C., Qin, K.Z., Sun, S., and Li, J.L., 2004, Paleozoic accretionary and collisional tectonics of the Eastern Tianshan (China): Implications for the continental growth of Central Asia: American Journal of Science, v. 304, p. 370–395. doi:10.2475/ajs.304.4.370

Xiong, X.L., Keppler, H., Audétat, A., Ni, H.W., Sun, W.D., and Li, Y.A., 2011, Partitioning of Nb and Ta between rutile and felsic melt and the fractionation of Nb/Ta during partial melting of hydrous metabasalt: Geochimica Et Cosmochimica Acta, v. 75, p. 1673–1692. doi:10.1016/j.gca.2010.06.039

Xu, X., Xia, L., Ma, Z., Wang, Y., Xia, Z., Li, X., and Wang, L., 2006, SHRIMP zircon U–Pb geochronology of the plagiogranites from Bayringou ophiolite in North Tianshan Mountains and the petrogenesis of the ophiolite: Acta Petrologica Sinica, v. 22, p. 83–94. [In Chinese with English abstract.]

Xu, Y., Mei, H., Xu, J., Huang, X., Wang, Y., and Chung, S.L., 2003, Origin of two differentiation trends in the Emeishan flood basalts: Chinese Science Bulletin, v. 48, p. 390–394.

Yan, Y.H., Xue, C.J., Zhang, Z.C., Ding, Z.X., Yang, W.H., and Han, Z.H., 2013, Geochemistry and genesis of the Qunjisayi

granite porphyry in the west of Awulale area, Western Tianshan Mountains: Acta Petrologica Et Mineralogica, v. 32, p. 139–153. [In Chinese with English abstract.]

Yang, W.-B., Niu, H.-C., Shan, Q., Chen, H.-Y., Hollings, P., Li, N.-B., Yan, S., and Zartman, R.E., 2014a, Geochemistry of primary-carbonate bearing K-rich igneous rocks in the Awulale Mountains, western Tianshan: Implications for carbon-recycling in subduction zone: Geochimica Et Cosmochimica Acta, v. 143, p. 143–164. doi:10.1016/j.gca.2014.04.033

Yang, W.-B., Niu, H.-C., Shan, Q., Luo, Y., Sun, W.-D., Li, C.-Y., Li, N.-B., and Yu, X.-Y., 2012, Late Paleozoic calc-alkaline to shoshonitic magmatism and its geodynamic implications, Yuximolegai area, western Tianshan, Xinjiang: Gondwana Research, v. 22, p. 325–340. doi:10.1016/j.gr.2011.10.008

Yang, W.-B., Niu, H.-C., Shan, Q., Sun, W.-D., Zhang, H., Li, N.-B., Jiang, Y.-H., and Yu, X.-Y., 2014b, Geochemistry of magmatic and hydrothermal zircon from the highly evolved Baerzhe alkaline granite: Implications for Zr-REE-Nb mineralization: Mineralium Deposita, v. 49, p. 451–470. doi:10.1007/s00126-013-0504-1

Zhang, H., Li, C.-Y., Yang, X.-Y., Sun, Y.-L., Deng, J.-H., Liang, H.-Y., Wang, R.-L., Wang, B.-H., Wang, Y.-X., and Sun, W.-D., 2014a, Shapinggou: The largest Climax-type porphyry Mo deposit in China: International Geology Review, v. 56, p. 313–331. doi:10.1080/00206814.2013.855363

Zhang, H., Ling, M.-X., Liu, Y.-L., Tu, X.-L., Wang, F.-Y., Li, C.-Y., Liang, H.-Y., Yang, X.-Y., Arndt, N.T., and Sun, W.-D., 2013a, High oxygen fugacity and slab melting linked to Cu mineralization: Evidence from Dexing porphyry copper deposits, Southeastern China: The Journal of Geology, v. 121, p. 289–305. doi:10.1086/669975

Zhang, L.F., Ai, Y.L., Li, X.P., Rubatto, D., Song, B., Williams, S., Song, S.G., Ellis, D., and Liou, J.G., 2007, Triassic collision of western Tianshan orogenic belt, China: Evidence from SHRIMP U-Pb dating of zircon from HP/UHP eclogitic rocks: Lithos, v. 96, p. 266–280. doi:10.1016/j.lithos.2006.09.012

Zhang, X., Klemd, R., Gao, J., Dong, L.-H., Wang, X.-S., Haase, K., Jiang, T., and Qian, Q., 2014b, Metallogenesis of the Zhibo and Chagangnuoer volcanic iron oxide deposits in the Awulale Iron Metallogenic Belt, Western Tianshan orogen, China: Journal of Asian Earth Sciences. doi:10.1016/j.jseaes.2014.06.004

Zhang, X., Tian, J., Gao, J., Klemd, R., Dong, L., Fan, J., Jiang, T., Hu, C., and Qian, Q., 2012a, Geochronology and geochemistry of granitoid rocks from the Zhibo syngenetic volcanogenic iron ore deposit in the Western Tianshan Mountains (NW China): Constraints on the age of mineralization and tectonic setting: Gondwana Research, v. 22, p. 585–596. doi:10.1016/j.gr.2011.06.007

Zhang, Y., Wang, Y., Geng, H., Zhang, Y., Fan, W., and Zhong, H., 2013b, Early Neoproterozoic (~850 Ma) back-arc basin in the Central Jiangnan Orogen (Eastern South China): Geochronological and petrogenetic constraints from meta-basalts: Precambrian Research, v. 231, p. 325–342. doi:10.1016/j.precamres.2013.03.016

Zhang, Z., Hou, T., Santosh, M., Li, H., Li, J., Zhang, Z., Song, X., and Wang, M., 2014c, Spatio-temporal distribution and tectonic settings of the major iron deposits in China: An overview: Ore Geology Reviews, v. 57, p. 247–263. doi:10.1016/j.oregeorev.2013.08.021

Zhang, Z., Mao, J., Saunders, A.D., Ai, Y., Li, Y., and Zhao, L., 2009, Petrogenetic modeling of three mafic–ultramafic layered intrusions in the Emeishan large igneous province, SW China, based on isotopic and bulk chemical constraints: Lithos, v. 113, p. 369–392. doi:10.1016/j.lithos.2009.04.023

Zhang, Z.C., Kang, J.L., Kusky, T., Santosh, M., Huang, H., Zhang, D.Y., and Zhu, J., 2012b, Geochronology, geochemistry and petrogenesis of Neoproterozoic basalts from Sugetbrak, northwest Tarim block, China: Implications for the onset of Rodinia supercontinent breakup: Precambrian Research, v. 220–221, p. 158–176. doi:10.1016/j.precamres.2012.08.002

Zhang, Z.H., Hong, W., Jiang, Z.S., Duan, S.G., Li, F.M., and Shi, F.P., 2014d, Geological characteristics and metallogenesis of iron deposits in western Tianshan, China: Ore Geology Reviews, V, v. 57, p. 425–440. doi:10.1016/j.oregeorev.2013.09.012

Zhao, Z.H., Bai, Z.H., Rui, Z.Y., Xiong, X.L., Mei, H.J., Wang, L.S., Wang, Y.X., and Bao, Z.W., 2000, Forecasting map of igneous rocks and mineralization in northern Western Tianshan. Project reports of 'Late Paleozoic volcanisms, shallow intrusive magmatism and Cu–Au polymetallic mineralization studies in northern West Tianshan'. [In Chinese.]

Zheng, J.P., Griffin, W.L., O'Reilly, S.Y., Zhang, M., Pearson, N., and Luo, Z.H., 2006, The lithospheric mantle beneath the southwestern Tianshan area, northwest China: Contributions to Mineralogy and Petrology, v. 151, p. 457–479. doi:10.1007/s00410-006-0071-x

Zhou, M.F., Robinson, P.T., Lesher, C.M., Keays, R.R., Zhang, C.J., and Malpas, J., 2005, Geochemistry, petrogenesis and metallogenesis of the Panzhihua gabbroic layered intrusion and associated Fe–Ti–V oxide deposits, Sichuan Province, SW China: Journal of Petrology, v. 46, p. 2253–2280. doi:10.1093/petrology/egi054

Zhu, Y., Zhang, L., Gu, L., Guo, X., and Zhou, J., 2005, The zircon SHRIMP chronology and trace element geochemistry of the Carboniferous volcanic rocks in western Tianshan Mountains: Chinese Science Bulletin, v. 50, p. 2201–2212. doi:10.1007/BF03182672

Zhu, Y.F., Guo, X., Song, B., Zhang, L.F., and Gu, L.B., 2009, Petrology, Sr–Nd–Hf isotopic geochemistry and zircon chronology of the Late Palaeozoic volcanic rocks in the southwestern Tianshan Mountains, Xinjiang, NW China: Journal of the Geological Society, v. 166, p. 1085–1099. doi:10.1144/0016-76492008-130

Zhu, Y.F., Zhou, J., and Guo, X., 2006a, Petrology and Sr-Nd isotopic geochemistry of the Carboniferous volcanic rocks in the western Tianshan Mountains, NW China: Acta Petrologica Sinica, v. 22, p. 1341–1350. [In Chinese with English abstract.]

Zhu, Y.F., Zhou, J., Song, B., Zhang, L.F., and Guo, X., 2006b, Age of the "Dahalajunshan" Formation in Xinjiang and its disintegration: Geology in China, v. 33, p. 487–497. [In Chinese with English abstract.]

Zindler, A., and Hart, S., 1986, Chemical geodynamics: Annual Review of Earth and Planetary Sciences, v. 14, p. 493–571. doi:10.1146/annurev.ea.14.050186.002425

Appendix

Table A1.   Zircon trace element abundance, Ce anomalies, and Ti-in-zircon temperatures.

Sample points	Age (Ma)	Ti	La	Ce	Pr	Nd	Sm	Eu	Gd	Tb	Dy	Ho	Er	Tm	Yb	T (°C)	$10^4/T$ (K^{-1})	δCe
Songhu rhyolite																		
SHZr-04	328	37.6	0.33	7.20	0.10	1.03	2.09	0.23	11.7	3.83	53.0	22.3	116	25.5	243	872	8.7	9.7
SHZr-08	328	7.10	0.03	6.70	0.08	1.09	2.26	0.43	14.7	4.83	67.8	26.5	138	30.0	296	712	10.2	31.7
SHZr-09	328	7.80	0.15	11.0	0.13	1.43	2.17	0.69	10.6	3.31	45.4	17.7	91	20.7	215	720	10.1	18.8
SHZr-11	328	20.9	0.14	8.40	0.14	1.02	2.05	0.13	8.40	3.36	45.7	19.8	100	23.3	221	810	9.2	14.5
SHZr-14	328	8.60	0.12	8.80	0.13	0.97	1.53	0.33	10.8	4.02	55.2	23.7	121	27.5	273	728	10.0	17.6
SHZr-16	328	10.6	0.03	5.70	0.05	0.56	1.30	0.41	11.8	3.94	53.2	21.3	114	25.9	250	747	9.8	38.9
SHZr-18	328	13.8	0.12	11.8	0.12	0.84	1.61	0.19	9.50	2.91	42.7	17.7	100	22.5	236	770	9.6	24.2
SHZr-19	328	11.1	0.08	8.10	0.07	0.76	1.32	0.32	12.0	4.45	66.2	26.3	143	31.7	335	750	9.8	27.0
SHZr-20	328	16.6	0.27	7.60	0.19	0.77	1.67	0.32	12.0	4.18	63.6	24.1	131	29.4	283	788	9.4	8.1
SHZr-21	328	7.80	0.16	6.60	0.09	0.72	1.29	0.25	9.50	3.83	54.8	22.2	116	27.5	268	720	10.1	13.3
SHZr-23	328	8.30	0.04	6.80	0.03	0.66	1.61	0.33	12.3	4.05	59.0	24.5	130	30.0	298	725	10.0	47.7
SHZr-24	328	11.0	0.39	8.10	0.15	1.59	1.51	0.35	11.0	3.51	53.8	21.1	112	25.0	260	749	9.8	8.1
SHZr-25	328	25.4	0.36	9.40	0.06	1.46	1.92	0.34	12.3	4.65	67.6	27.2	143	32.0	317	830	9.1	15.1
Songhu tuff																		
SH1-1-01	305	17.3	0.64	8.50	0.34	0.95	\	\	4.20	1.20	16.8	6.60	36	8.3	81	792	9.4	4.5
SH1-1-02	305	34.0	2.59	9.90	0.55	3.32	4.24	0.52	20.2	6.87	83.5	30.4	146	28.4	255	861	8.8	2.0
SH1-1-03	305	24.0	0.95	10.4	0.40	3.53	3.18	1.01	17.3	5.39	65.2	24.4	115	23.9	206	824	9.1	4.2
SH1-1-05	305	39.8	0.98	35.7	0.26	3.73	7.92	1.35	36.9	11.4	136	48.7	221	41.6	363	879	8.7	17.4
SH1-1-06	305	24.8	4.10	20.1	1.16	6.94	3.73	0.74	19.2	5.73	80.6	29.9	143	28.5	261	828	9.1	2.3
SH1-1-08	305	19.3	0.72	27.1	0.33	3.55	4.57	0.62	22.1	6.65	89.7	32.2	156	31.8	302	802	9.3	13.6
SH1-1-10	305	54.3	9.47	33.5	3.24	13.2	7.01	0.95	23.0	6.00	78.4	30.9	146	29.0	251	915	8.4	1.5
SH1-1-11	305	23.1	4.09	23.7	1.22	7.47	4.59	1.25	30.4	8.85	124	41.7	214	38.3	355	820	9.1	2.6
SH1-1-12	305	145	3.27	8.90	0.75	1.77	2.12	0.36	8.40	2.63	35.5	13.3	60	12.2	114	1048	7.6	1.4
SH1-1-13	305	52.0	0.80	14.7	0.31	3.13	4.92	1.03	18.1	6.32	81.0	29.8	130	26.8	232	910	8.5	7.3
SH1-1-15	305	44.0	1.52	12.9	1.07	2.93	\	0.30	9.40	2.45	37.8	15.0	74	16.0	132	891	8.6	2.5
Yuximolegai quartz syenite porphyry																		
YXQ-01	284	3.60	0.06	9.20	0.10	1.63	2.53	0.86	13.2	4.46	53.4	21.2	99	22.3	215	658	10.7	28.0
YXQ-02	284	20.9	0.42	16.8	0.57	7.49	11.13	0.46	45.4	14.4	155	55.4	243	50.6	463	810	9.2	8.5
YXQ-03	284	25.0	1.17	31.2	0.78	6.31	7.11	0.79	28.7	9.18	103	38.4	181	40.3	379	829	9.1	8.0
YXQ-04	284	37.8	3.83	42.1	2.07	12.7	7.95	1.54	25.5	7.49	83.9	30.2	138	30.3	301	873	8.7	3.7
YXQ-05	284	17.8	0.61	30.5	0.65	7.02	9.89	0.81	42.6	12.5	135	49.8	220	48.8	448	794	9.4	11.9
YXQ-06	284	28.6	1.33	32.8	0.75	7.98	7.26	0.92	27.9	8.83	98.5	36.7	175	37.8	362	843	9.0	8.1
YXQ-07	284	63.5	3.49	73.2	2.40	15.1	12.41	2.48	42.5	12.6	132	46.6	205	44.7	422	935	8.3	6.2
YXQ-08	284	76.1	2.51	15.1	0.62	4.47	4.59	0.18	19.1	6.17	72.3	26.9	124	28.2	266	958	8.1	3.0
YXQ-09	284	21.7	0.87	32.5	0.92	10.16	13.33	0.89	53.2	16.2	174	63.2	273	58.1	516	814	9.2	8.9
YXQ-10	284	19.9	6.22	44.6	4.55	8.69	6.90	0.73	19.9	6.61	73.9	27.7	132	29.6	297	805	9.3	2.1
YXQ-11	284	118	13.18	88.2	6.84	39.6	26.13	6.59	66.0	18.2	184	60.6	262	53.9	505	1018	7.7	2.3
YXQ-12	284	116	10.99	60.3	4.62	28.1	16.13	6.71	45.6	12.6	125	44.4	195	42.6	407	1015	7.8	2.1
YXQ-13	284	106	15.30	82.7	4.98	26.1	19.08	3.92	62.5	17.1	178	64.4	278	58.0	524	1003	7.8	2.3
YXQ-14	284	16.9	0.07	10.6	0.18	2.68	4.90	0.19	24.1	8.64	95.4	36.9	170	37.0	352	789	9.4	22.6
YXQ-15	284	40.0	1.15	14.8	0.73	7.91	12.07	0.42	51.4	16.0	171	61.6	264	55.7	506	880	8.7	3.9
YXQ-16	284	20.4	1.15	16.9	0.72	5.92	4.28	0.99	13.4	4.15	40.9	15.9	75	16.7	165	808	9.3	4.6
YXQ-17	284	21.8	0.33	26.7	0.66	9.40	14.90	0.66	62.5	18.2	190	68.0	289	60.2	547	815	9.2	14.1
YXQ-18	284	34.5	0.85	20.4	0.64	4.37	4.48	0.47	18.8	6.26	76.2	29.4	134	30.2	293	863	8.8	6.8
YXQ-19	284	19.1	0.38	18.6	0.41	6.02	7.69	0.33	35.4	10.9	120	45.2	204	42.9	394	801	9.3	11.5
YXQ-20	284	17.0	0.60	54.4	0.93	8.49	10.23	0.79	40.4	12.4	136	49.0	210	44.2	404	790	9.4	17.8
YXQ-21	284	42.1	3.47	38.6	1.37	9.85	10.36	1.32	39.0	11.6	126	47.0	208	43.4	405	885	8.6	4.3
YXQ-22	284	36.2	2.07	26.4	1.06	10.0	11.78	1.29	45.1	13.6	147	52.7	229	49.0	443	868	8.8	4.4
YXQ-23	284	109	5.40	41.7	1.78	10.0	7.51	1.25	24.1	7.15	77.1	28.1	130	29.5	287	1006	7.8	3.3
YXQ-24	284	34.9	2.33	25.4	1.52	14.9	12.85	1.09	45.3	13.6	150	53.6	241	52.7	484	864	8.8	3.3
YXQ-25	284	38.4	0.30	15.3	0.26	2.77	5.05	0.31	24.8	7.36	84.8	31.3	144	31.8	306	875	8.7	13.3
YXQ-26	284	42.1	1.36	18.8	1.27	9.91	10.78	0.73	48.9	14.3	165	60.2	277	59.7	543	885	8.6	3.5
YXQ-28	284	23.4	0.78	16.9	0.82	10.1	15.10	0.79	69.6	20.1	215	78.1	334	67.6	619	822	9.1	5.2
YXQ-29	284	16.7	2.42	57.1	1.48	10.4	7.54	0.99	18.6	5.54	59.1	21.8	100	21.7	231	788	9.4	7.4
YXQ-30	284	31.0	0.85	20.5	0.50	4.73	5.89	0.42	21.1	6.91	76.8	30.2	140	32.9	318	851	8.9	7.7

(*Continued*)

Table A1. (Continued).

Sample points	Age (Ma)	Ti	La	Ce	Pr	Nd	Sm	Eu	Gd	Tb	Dy	Ho	Er	Tm	Yb	T (°C)	$10^4/T$ (K^{-1})	δCe
Chagangnuoer dacite																		
09CGB-1B-04	313	9.60	0.34	10.9	0.25	2.03	3.77	0.71	22.4	8.63	112	46.8	222	49.0	475	738	9.9	9.2
09CGB-1B-09	313	8.30	29.89	88.7	11.91	64.6	19.02	2.59	42.6	11.9	132	51.4	234	49.9	465	725	10.0	1.2
09CGB-1B-11	313	3.90	0.03	5.00	0.08	1.19	3.51	0.80	20.5	7.08	89.0	37.4	175	37.8	352	665	10.7	25.8
09CGB-1B-12	313	85.7	4.02	35.4	1.24	7.23	4.42	0.60	23.7	9.22	125	53.9	280	65.1	660	973	8.0	3.9
09CGB-1B-15	313	7.30	1.58	11.0	0.62	4.38	3.08	0.64	16.4	5.79	79.9	34.4	173	38.7	389	714	10.1	2.7
09CGB-1B-16	313	5.90	0.57	18.6	0.40	5.47	9.68	2.06	57.4	20.1	243	94.8	426	88.1	795	697	10.3	9.5
09CGB-1B-17	313	12.2	8.00	47.7	2.93	16.7	12.28	2.73	46.7	14.5	162	58.4	254	52.5	474	759	9.7	2.4
09CGB-1B-23	313	94.6	2.26	31.1	0.75	5.70	7.30	1.53	48.5	17.9	226	92.2	404	88.8	769	986	7.9	5.8
09CGB-1B-24	313	16.2	0.23	6.40	0.18	1.78	3.25	0.85	21.0	7.65	95.2	39.7	186	40.5	387	785	9.5	7.7
09CGB-1B-26	313	12.8	0.54	7.80	0.27	2.20	3.04	0.57	18.7	6.96	89.0	39.1	190	43.3	433	763	9.7	5.0
09CGB-1B-31	313	19.9	0.13	7.30	0.15	4.38	4.75	1.76	29.9	9.44	119	49.2	243	55.8	562	805	9.3	13.0
09CGB-1B-32	313	4.00	0.09	9.20	0.30	3.41	6.08	2.40	36.3	12.6	161	66.2	317	72.6	723	667	10.6	14.1
09CGB-1B-34	313	5.50	2.68	15.0	1.05	6.33	3.26	0.83	17.4	6.63	87.8	38.8	192	44.0	426	691	10.4	2.2
Chagangnuoer ferrobasalts																		
CGB2-1	314	6.00	0.49	24.3	0.47	5.83	10.62	2.39	56.4	21.4	261	104	477	102.9	1006	697	10.3	12.4
CGB2-3	314	25.0	0.62	32.2	0.27	4.33	12.12	1.29	70.8	25.6	329	133	614	132.9	1218	829	9.1	19.3
CGB2-4	314	15.0	0.27	8.70	0.23	2.05	3.35	0.79	23.9	8.77	117	51.6	235	51.8	503	778	9.5	8.6
CGB2-5	314	9.20	0.69	8.10	0.21	1.84	2.91	0.49	15.5	6.22	77.2	33.8	161	35.6	360	734	9.9	5.2
CGB2-6	314	6.50	0.31	7.70	0.26	2.13	3.54	1.16	25.4	9.99	130	54.1	249	55.8	539	704	10.2	6.6
CGB2-7	314	6.00	0.17	5.10	0.14	1.30	2.49	0.76	19.2	7.33	95.7	39.7	190	40.6	402	699	10.3	8.0
CGB2-9	314	10.4	0.16	5.90	0.13	1.04	1.63	0.51	14.0	5.35	74.0	31.5	154	34.6	346	744	9.8	9.8
CGB2-10	314	13.8	0.38	9.50	0.29	3.56	3.68	1.13	24.7	9.20	123	53.9	260	57.0	563	770	9.6	7.0